Imprint of chaos on the ocean energy cycle from an eddying North Atlantic ensemble

Takaya Uchida, FSU (tuchida@fsu.edu)
Quentin Jamet, INRIA (quentin.jamet@inria.fr)
William K. Dewar, FSU (wdewar@fsu.edu)
Bruno Deremble, CNRS (bruno.deremble@cnrs.fr)
Andrew C. Poje, CUNY (andrewpoje@gmail.com)
Luolin Sun, CNRS (luolin.sun@univ-grenoble-alpes.fr)

Imprint of chaos on the ocean energy cycle from an eddying North Atlantic ensemble

Takaya Uchida[a,b] , Quentin Jamet[b,c] , William K. Dewar[b,d] , Bruno Deremble[b] , Andrew C. Poje[e] & Luolin Sun[b]

[a] *Center for Ocean-Atmospheric Prediction Studies, Florida State University, Florida, USA*

[b] *Université Grenoble Alpes, CNRS, INRAE, IRD, Grenoble-INP, Institut des Géosciences de l'Environnement, Grenoble, France*

[c] *INRIA, ODYSSEY group, Ifremer, Plouzané, France*

[d] *Department of Earth, Ocean and Atmospheric Science, Florida State University, Florida, USA*

[e] *Department of Mathematics, College of Staten Island, The City University of New York, New York, USA*

Corresponding author: Takaya Uchida, tuchida@fsu.edu

ABSTRACT: We examine the ocean energy cycle where the eddies are defined about the ensemble mean of a partially air-sea coupled, eddy-rich ensemble simulation of the North Atlantic. The decomposition about the ensemble mean leads to a parameter-free definition of eddies, which is interpreted as the expression of oceanic chaos. Using the ensemble framework, we define the reservoirs of mean and eddy kinetic energy (MKE and EKE respectively) and mean total dynamic enthalpy (MTDE). We opt for the usage of dynamic enthalpy (DE) as a proxy for potential energy due to its dynamically consistent relation to hydrostatic pressure in Boussinesq fluids and non-reliance on any reference stratification. The curious result that emerges is that the potential energy reservoir cannot be decomposed into its mean and eddy components, and the eddy flux of DE can be absorbed into the EKE budget as pressure work. We find from the energy cycle that while baroclinic instability, associated with a positive vertical eddy buoyancy flux, tends to peak around February, EKE takes its maximum around September in the wind-driven gyre. Interestingly, the energy input from MKE to EKE, a process sometimes associated with barotropic processes, becomes larger than the vertical eddy buoyancy flux towards the summer and autumn. Our results question the common notion that the inverse energy cascade of winter-time EKE energized by baroclinic instability within the mixed layer is solely responsible for the summer-to-autumn peak in EKE, and suggest that the non-local eddy transport of DE and local transfer of energy from MKE to EKE could also contribute to the seasonal EKE maxima.

1. Introduction

There has been much interest in the recent decades on Earth's climate sensitivity, the long-term thermal response to an increase in atmospheric carbon dioxide (Sherwood et al. 2020), motivated by the fact that our emission of anthropogenic carbon since the industrial revolution may be the culprit for a warming climate (Masson-Delmotte et al. 2021). Nonetheless, significant uncertainties persist in the climate sensitivity and have not been reduced since the Charney Report published in 1979 (Charney et al. 1979; Knutti et al. 2017). In understanding and quantifying the climate system, a useful framework has been to examine the energy pathways, which elucidates how much of the incoming solar radiation gets retained and redistributed around the Earth system to warm or cool the climate (Hartmann et al. 1986).

Amongst the Earth system components, the ocean is perhaps the most significant reservoir of energy on centennial to millennial timescales due to its large heat capacity and density, and capability to dissolve and store carbon and salts. In a seminal work, Wunsch and Ferrari (2004) attempted to provide an overview of the energy pathways for the oceans but came short in one crucial aspect: The role of mesoscale eddies as a conduit between the wind-driven general circulation and small-scale three-dimensional isotropic turbulence. Our lack of understanding on how mesoscale eddies interact with dynamics associated with other scales hinders our ability to predict the future climate due to their disproportionately large role in globally transporting heat and carbon (Griffies et al. 2015; Gnanadesikan et al. 2015).

One of the difficulties in quantifying the impact of mesoscale eddies lies in the identification of the eddies themselves (Wunsch 1981), which exist in a soup of anisotropic and inhomogeneous flows (Uchida et al. 2021c, 2023b). For practical reasons, eddies have often been defined via a Reynold's decomposition about a spatial and/or temporal coarse graining (e.g. Bachman et al. 2015; Aiki et al. 2016; Aoki et al. 2016; Uchida et al. 2017; Demyshev and Dymova 2022; Buzzicotti et al. 2023; Xie et al. 2023); this always leaves the question: How sensitive are the results to their method of eddy-mean flow decomposition? Aiki and Richards (2008) demonstrated that by adjusting the temporal window over which the mean was taken, the amount of kinetic and potential energy stored in the mean and eddy reservoirs could change by up to a factor of four. More recently, Demyshev and Dymova (2022) showed complementary results that depending on the time frame over which the averaging is taken to define the mean flow, the relative significance of energy pathways to the eddy kinetic energy (EKE) reservoir changed. As one may imagine, the amount of energy stored in each reservoir and exchanged amongst them is also dependent on the spatial scale taken for the decomposition (Loose et al. 2022).

Here, we take a different approach by running an ensemble of 'eddy-rich' simulations of the North Atlantic ocean using the Massachusetts Institute of Technology general circulation model (MITgcm; Marshall et al. 1997) and decompose the flow about the ensemble mean. This leads to a parameter-free definition of eddies where the mean flow can be interpreted as the oceanic response to the common atmospheric state and eddies as the expression of oceanic chaos and intrinsic variability (e.g. Chen and Flierl 2015; Sérazin et al. 2017; Leroux et al. 2018; Uchida et al. 2021a). The ensemble approach has some history in the atmospheric and climate literature focusing on the dynamics and process-oriented studies (e.g. Sui et al. 1994; Lenderink et al. 2007; Nikiéma and Laprise 2013; Hersbach et al. 2015; Xie et al. 2016; Romanou et al. 2023) but is still relatively novel in the field of oceanography (Uchida et al. 2022b; Jamet et al. 2022).

With this definition of mean flow and eddies, we will diagnose the ocean energy cycle with an emphasis on the interaction between the kinetic and potential energy reservoirs (Lorenz 1955; Bleck 1985). Furthermore, we will adopt a definition of potential energy which does not depend on a reference state of stratification and is dynamically and thermodynamically consistent with the equations being solved. As we shall see, the energy cycle that emerges differs from the canonical Lorenz energy cycle primarily in that the energy reservoir corresponding to eddy available potential energy (APE) does not explicitly appear and the mean total potential energy reservoir directly interacts with the eddy kinetic energy (EKE) reservoir.

The paper is organized as follows: In Section 2, we provide a brief description of the simulation and an overview on the energy cycle. Results are given in Section 3 and we provide a summary in Section 4.

2. Methods

a. Model description

We use model outputs from a recently developed 48-member eddy-rich ($1/12°$) ensemble of the North Atlantic (Jamet et al. 2019) partially air-sea coupled via the Cheap Atmospheric Mixed Layer model (CheapAML; Deremble et al. 2013). As our model domain is focused on the North Atlantic, the basin was configured to wrap around zonally in order to save memory allocation (e.g. Fig. 3). The dataset has been used to quantify the effect of oceanic chaos on the Atlantic Meridional Overturning Circulation (Jamet et al. 2019, 2020c; Dewar et al. 2022), and spatial variability of eddies, here defined about the ensemble mean and interpreted as the expression of oceanic chaos (Uchida et al. 2021c, 2022b, 2023a,b). In this study, we shift our attention to the temporal variability by examining the energy cycle. The ensemble mean, being orthogonal to the spatiotemporal dimensions, commutes with the space-and-time derivatives and maintains the desirable statistical properties of non-stationarity and inhomogeneity upon a Reynold's decomposition. We use data from the year 1967 where ensemble outputs from the MITgcm `diagnostics` package are saved as instantaneous snapshots every five days, which allows us to close the total (mean + eddy) momentum budgets to machine precision. In other words, our analysis is somewhat restricted by the available model outputs in closing the budget. The kinetic energy (KE) budgets are subsequently constructed by taking the dot product between the horizontal momentum vector and each term in the momentum equations (cf. Appendix).

b. Ocean energy cycle

The mean total kinetic energy (MTKE; $\langle|\boldsymbol{u}|^2\rangle/2$) can be decomposed into its mean and eddy kinetic energy (MKE and EKE) reservoirs as

$$K^{\#} \stackrel{\text{def}}{=} |\langle\boldsymbol{u}\rangle|^2/2, \tag{1}$$

$$\langle\mathscr{K}\rangle \stackrel{\text{def}}{=} \langle|\boldsymbol{u}'|^2\rangle/2, \tag{2}$$

where $\boldsymbol{u} = u\hat{\boldsymbol{x}} + v\hat{\boldsymbol{y}}$ is the horizontal momentum vector, $\hat{\boldsymbol{x}}$ and $\hat{\boldsymbol{y}}$ are the zonal and meridional unit vectors respectively, $\langle\cdot\rangle$ is the ensemble mean operator and $(\cdot)' \stackrel{\text{def}}{=} (\cdot) - \langle\cdot\rangle$, $\langle(\cdot)'\rangle = 0$. Regarding potential energy, while many possible ways to define it in oceanic primitive equations have been proposed (e.g. Aiki and Richards 2008; Molemaker and McWilliams 2010; Nycander 2010; Von Storch et al. 2012; Saenz et al. 2015; Tailleux 2013, 2016; Dewar et al. 2016; Aiki et al. 2016; Kang et al. 2016; Guo et al. 2022; Yang et al. 2022; Loose et al. 2022; Demyshev and Dymova 2022; Tailleux and Wolf 2023; Yang et al. 2023), defining a 'reference' stratification in realistic simulations has remained subjective primarily due to the non-linear equation of state (EOS) for seawater. The prescription of such reference state, furthermore, hinders the dynamical and thermodynamical consistency with the equations of motion being solved for a Boussinesq seawater. Namely, buoyancy (or density anomaly in defining buoyancy) must satisfy the hydrostatic pressure relation while remaining a thermodynamical function when considering the energetics. We opt for dynamic enthalpy (DE; Young 2010), which is a, if not 'the', natural extension of gravitational potential energy with a non-linear EOS, and does not depend on a reference state

$$\tilde{h}(\Theta, S, \Phi) = \int_{\Phi_0}^{\Phi} \frac{\tilde{b}(\Theta, S, \Phi^*)}{g} \, d\Phi^* \left(= \int_z^0 b \, dz^* \right), \tag{3}$$

where $\Phi = \Phi_0 - gz$ is the static dynamically non-active part of hydrostatic pressure, the superscript * indicates a dummy variable, and $\tilde{(\cdot)}$ denotes a thermodynamical function. Following Young (2010), the tilde notation distinguishes thermodynamic functions from fields in space-time, viz. $\tilde{b}(\Theta, S, \Phi) = b(t, z, y, x)$. Θ and S are potential temperature and practical salinity, $\tilde{b} = -g\frac{\tilde{\rho}-\rho_0}{\rho_0}$ is buoyancy, $\tilde{\rho}$ density based on Jackett and McDougall (1995), $\rho_0 = 999.8\,\mathrm{kg\,m^{-3}}$ the reference density prescribed in MITgcm, and g gravity. Although buoyancy in Young (2010) was defined as $\tilde{b} = -g\frac{\tilde{\rho}-\rho_0}{\tilde{\rho}}$, we make use of the former convention for simplicity (particularly when taking its partial derivatives) and will neglect the small differences that emerge between the two (cf. Eden 2015). We emphasize that the integration in (3) is taken by fixing Θ and S in respect to $\Phi(z)$, e.g. $\Theta = \Theta(t, z, y, x)$. The term on the right-hand side of (3) in parentheses shows the integration by substituting Φ with z in space-time.

As detailed in the Appendix, the evolution equations for MKE and EKE are

$$\frac{D^\#}{Dt} K^\# = -\big\langle \boldsymbol{v}' \cdot \nabla(\langle \boldsymbol{u} \rangle \cdot \boldsymbol{u}') \big\rangle - \langle \boldsymbol{v} \rangle \cdot \nabla \langle \phi \rangle + \langle w \rangle \langle b \rangle + \langle \boldsymbol{v}'\boldsymbol{u}' \rangle \cdot \nabla \langle \boldsymbol{u} \rangle + \langle \boldsymbol{u} \rangle \cdot \langle \boldsymbol{\mathcal{X}} \rangle, \tag{4}$$

$$\frac{D^\#}{Dt} \langle \mathscr{K} \rangle = -\langle \boldsymbol{v}' \cdot \nabla \mathscr{K} \rangle - \langle \boldsymbol{v}' \cdot \nabla \phi' \rangle + \langle w' b' \rangle - \langle \boldsymbol{u}'\boldsymbol{v}' \rangle \cdot \nabla \langle \boldsymbol{u} \rangle + \langle \boldsymbol{u}' \cdot \boldsymbol{\mathcal{X}}' \rangle, \tag{5}$$

respectively where $\frac{D^\#}{Dt} \stackrel{\text{def}}{=} \frac{\partial}{\partial t} + \langle \boldsymbol{v} \rangle \cdot \nabla$ is the mean Lagrangian tendency, $\boldsymbol{v} = \boldsymbol{u} + w\hat{\boldsymbol{z}}$ the non-divergent three-dimensional momentum vector, ϕ the dynamically active part of hydrostatic pressure, and $\boldsymbol{\mathcal{X}} \, (= \boldsymbol{\mathcal{F}} + \varepsilon)$ is the net non-conservative term consisting of forcing, viscous dissipation and contribution from the K-Profile Parametrization (KPP; Large et al. 1994) to the momentum equations.

On the other hand, ensemble averaging the Lagrangian tendency of total dynamic enthalpy (TDE; (A6)) under adiabatic conditions is

$$\frac{D^{\#}}{Dt}\langle h\rangle + \langle \boldsymbol{v}' \cdot \nabla h' \rangle = \left\langle \frac{D}{Dt} h \right\rangle = -\langle w\rangle\langle b\rangle - \langle w'b'\rangle \,. \tag{6}$$

Since DE is a thermodynamical function, the mean Lagrangian tendency of mean total dynamic enthalpy (MTDE; $\langle h\rangle$) can also be expressed as

$$\begin{aligned}\frac{D^{\#}}{Dt}\langle h\rangle = \left\langle \frac{D^{\#}}{Dt} h \right\rangle &= \langle \tilde{h}_{\Phi}\rangle \frac{D^{\#}}{Dt}\Phi + \left\langle \tilde{h}_{\Theta} \frac{D^{\#}}{Dt}\Theta \right\rangle + \left\langle \tilde{h}_{S} \frac{D^{\#}}{Dt} S \right\rangle \\ &= -\langle w\rangle\langle b\rangle + \mathcal{H} \,, \end{aligned} \tag{7}$$

where $\mathcal{H} \overset{\text{def}}{=} \left\langle \tilde{h}_{\Theta} \frac{D^{\#}}{Dt}\Theta \right\rangle + \left\langle \tilde{h}_{S} \frac{D^{\#}}{Dt} S \right\rangle$ encapsulates the chain rule in respect to potential temperature and practical salinity, and is proportional to their eddy flux and diabatic, molecular and non-hydrostatic effects. The latter three effects are generally ignored hereon; adiabadicity is assumed for the thermodynamics as the tendency terms for temperature and salinity were not saved as model outputs. The subscripts $(\cdot)_{\Phi}$, $(\cdot)_{\Theta}$ and $(\cdot)_{S}$ denote partial derivatives in thermodynamics. Subtracting (7) from (6) leaves us with the identity

$$\langle \boldsymbol{v}' \cdot \nabla h' \rangle = -\langle w'b'\rangle - \mathcal{H} \,. \tag{8}$$

A subtle difference between MTKE and MTDE is that the former is quadratic while the latter is a single-order variable, yet both have the dimension of energy; MTDE cannot be explicitly decomposed into its mean and eddies like MTKE. In the quasi-geostrophic sense, MTDE is the combined reservoir of mean and eddy available potential energy (APE). Nonetheless, (4) - (6) form a complete set of equations to describe the energy cycle in primitive equations. The problem arises, however, that $\langle \tilde{b}\rangle$ and $\langle \tilde{h}\rangle$ are no longer thermodynamical functions for a non-linear EOS, and consequently nor are b' and h'. In other words, the energy cycle loses its direct ties with the thermodynamics.

We can make further progress by appealing to the approximation that second- and higher-order terms of thermodynamics are negligible, viz. $\langle \tilde{b} \rangle = \widetilde{\overline{b}} + \widetilde{\mathscr{B}}$,

$$\langle \tilde{h} \rangle = \int_{\Phi_0}^{\Phi} \frac{\widetilde{\overline{b}} + \widetilde{\mathscr{B}}}{g} \, d\Phi^* \simeq \widetilde{H} \, . \tag{9}$$

$\widetilde{H} \overset{\text{def}}{=} g^{-1} \int_{\Phi_0}^{\Phi} \widetilde{\overline{b}} \, d\Phi^*$ where $\widetilde{\overline{b}} \overset{\text{def}}{=} \tilde{b}(\langle \Theta \rangle, \langle S \rangle, \Phi)$ is buoyancy given the mean potential temperature and practical salinity, and the non-linearity in EOS shouldered by $\widetilde{\mathscr{B}}$, which is second order in temperature and salinity fluctuations at most, is ignored (cf. (A9) and Fig. A2). In view of (9), (8) can be simplified as

$$\langle w' b^{\dagger} \rangle \simeq -\langle \boldsymbol{v}' \cdot \nabla h^{\dagger} \rangle + \widetilde{H}_{\langle \Theta \rangle} \langle \boldsymbol{v}' \cdot \nabla \Theta' \rangle + \widetilde{H}_{\langle S \rangle} \langle \boldsymbol{v}' \cdot \nabla S' \rangle \, , \tag{10}$$

where $\tilde{b}^{\dagger} \overset{\text{def}}{=} \tilde{b} - \widetilde{\overline{b}}$ $(\simeq b')$ and $\tilde{h}^{\dagger} \overset{\text{def}}{=} \tilde{h} - \widetilde{H}$ $(\simeq h')$ for the remainder of this manuscript (cf. (A14) and Fig. A3). Following through with the linear approximation and plugging (10) into (A5) and (6) allows us to reformulate the evolution equations of MKE, EKE and MTDE as

$$K^{\#}_t + \langle \boldsymbol{v} \rangle \cdot \nabla K^{\#} \simeq -\langle \boldsymbol{v} \rangle \cdot \nabla \overline{\phi} + \underbrace{\langle w \rangle \overline{b}}_{=H_{\leftrightarrow} K^{\#}} - \nabla \cdot \big\langle \boldsymbol{v}' (\langle \boldsymbol{u} \rangle \cdot \boldsymbol{u}') \big\rangle + \underbrace{\langle \boldsymbol{v}' \boldsymbol{u}' \rangle \cdot \nabla \langle \boldsymbol{u} \rangle}_{=-K^{\#}_{\leftrightarrow} \mathscr{K}} + \langle \boldsymbol{u} \rangle \cdot \langle \boldsymbol{\mathcal{X}} \rangle \, , \tag{11}$$

$$\begin{aligned} \langle \mathscr{K} \rangle_t + \langle \boldsymbol{v} \rangle \cdot \nabla \mathscr{K} \simeq -\big\langle \boldsymbol{v}' \cdot \nabla (\phi^{\dagger} + \mathscr{K} + h^{\dagger}) \big\rangle \underbrace{- \langle \boldsymbol{v}' \boldsymbol{u}' \rangle \cdot \nabla \langle \boldsymbol{u} \rangle}_{=K^{\#}_{\leftrightarrow} \mathscr{K}} + \langle \boldsymbol{u}' \cdot \boldsymbol{\mathcal{X}}' \rangle \\ \underbrace{+ \widetilde{H}_{\langle \Theta \rangle} \langle \boldsymbol{v}' \cdot \nabla \Theta' \rangle + \widetilde{H}_{\langle S \rangle} \langle \boldsymbol{v}' \cdot \nabla S' \rangle}_{=H_{\leftrightarrow} \mathscr{K}} \, , \end{aligned} \tag{12}$$

and

$$H_t + \langle \boldsymbol{v} \rangle \cdot \nabla H \simeq \underbrace{-\langle w \rangle \overline{b}}_{=-H_{\leftrightarrow} K^{\#}} \underbrace{- \Big(\widetilde{H}_{\langle \Theta \rangle} \langle \boldsymbol{v}' \cdot \nabla \Theta' \rangle + \widetilde{H}_{\langle S \rangle} \langle \boldsymbol{v}' \cdot \nabla S' \rangle \Big)}_{=-H_{\leftrightarrow} \mathscr{K}} \, , \tag{13}$$

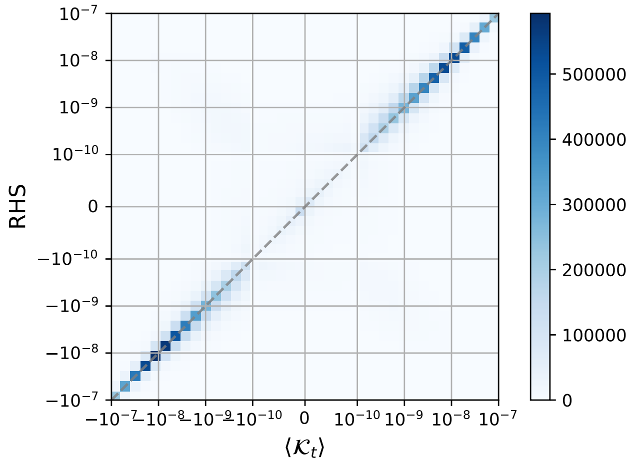

FIG. 1. Joint histogram of $\langle \mathscr{K}_t \rangle$ and the sum of other terms in (12). The histogram was computed for January 1, 1967 over the entire three-dimensional domain of the ensemble output. A one-to-one line is shown as the grey dashed line. The histogram was computed using the `xhistogram` Python package (Abernathey et al. 2021b).

respectively where $\overline{b}(t,z,y,x) = \overline{\tilde{b}} = \tilde{b}(\langle\Phi\rangle,\langle S\rangle,\Phi)$, $\overline{\phi}_z \stackrel{\text{def}}{=} \overline{b}$ $(\simeq \langle\phi_z\rangle)$ and $\phi_z^\dagger \stackrel{\text{def}}{=} b^\dagger$ $(\simeq \phi_z')$ and the subscripts $(\cdot)_t$ and $(\cdot)_z$ denote partial derivatives in space-time. The curious, and interesting, aspect of (12) is that the full statement of generalized energy flux now involves fluctuations of DE and the dynamically active part of hydrostatic pressure $-\langle\nabla\cdot[\boldsymbol{v}'(\phi^\dagger + h^\dagger)]\rangle$, and these are quantities that can drive cross-scale energy transfers (upon neglecting the non-linearities in EOS). The energy cycle with full consideration of a non-linear EOS and diabatic terms is derived in the Appendix. A joint histogram demonstrates that (12) holds relatively well considering the simplifications we have made to the thermodynamics (Fig. 1).

With the energy reservoirs defined, we can express the energy exchanges amongst the reservoirs. The exchange between MKE and EKE ($K^\#_\leftrightarrow\mathscr{K}$), MTDE and MKE ($H_\leftrightarrow K^\#$), and MTDE and EKE ($H_\leftrightarrow\mathscr{K}$) reservoirs, which are non-zero upon a global volume integration, are

$$K^\#_\leftrightarrow\mathscr{K} \stackrel{\text{def}}{=} -\big(\langle u'\boldsymbol{v}'\rangle\cdot\nabla\langle u\rangle + \langle v'\boldsymbol{v}'\rangle\cdot\nabla\langle v\rangle\big)\,, \tag{14}$$

$$H_\leftrightarrow K^\# \stackrel{\text{def}}{=} \langle w\rangle\overline{b}\left(= \widetilde{H}_\Phi\frac{D^\#}{Dt}\Phi \simeq \langle w\rangle\langle b\rangle\right)\,, \tag{15}$$

$$H_\leftrightarrow\mathscr{K} \stackrel{\text{def}}{=} \widetilde{H}_{\langle\Theta\rangle}\langle\boldsymbol{v}'\cdot\nabla\Theta'\rangle + \widetilde{H}_{\langle S\rangle}\langle\boldsymbol{v}'\cdot\nabla S'\rangle\ \left(\simeq \langle w'b^\dagger\rangle + \langle\boldsymbol{v}'\cdot\nabla h^\dagger\rangle\right)\,, \tag{16}$$

as indicated from (11) - (13). Unlike the canonical Lorenz energy cycle (Lorenz 1955; Uchida et al. 2021b), notice that there is no term corresponding to the exchange with the mean and eddy APE reservoirs but rather that MTDE directly interacts with the MKE and EKE reservoirs (Fig. 2). The term $\langle \boldsymbol{v}' \cdot \nabla h^\dagger \rangle$, which would seemingly identify as the exchange between mean and eddy APE reservoirs, gets directly passed onto EKE with the DE fluctuation serving as its conduit and retains no energy as $h^\dagger$ (i.e $\langle h^\dagger \rangle \simeq 0$). Furthermore, (12) demonstrates that the eddy flux divergence of EDE can be consolidated as pressure work, which leaves us with the effect of eddy temperature and salinity flux in (16). Figure A3 exhibits that (16) approximately holds throughout the domain. We argue that this deviation from the Lorenz cycle of a non-explicit eddy APE reservoir results from the fact that quasi geostrophy corresponds to the thickness-weighted primitive equations of motion in isopycnal coordinates, and not the unweighted equations in geopotential coordinates. Under quasi geostrophy, the isopycnal layer thickness is constant, leading to quasi-geostrophic (QG) variables being implicitly thickness-weighted averaged (Marshall et al. 2012; Maddison and Marshall 2013; Uchida et al. 2023a; Meunier et al. 2023). Nonetheless, an energy budget can be formulated for non-thickness weighted primitive equations under geopotential coordinates (cf. (11) - (13) and Appendix; Eden 2015) so we proceed in examining the energy cycle under this formalism.

3. Results

We start by showing the winter and summertime MKE, EKE and MTDE vertically averaged over the surface 1000 m, a depth over which the wind-driven gyre is roughly contained (Jamet et al. 2020b). The Gulf Stream, Gulf of Mexico Loop Current, Equatorial Under Current and North Brazil Current are apparent in MKE (Fig. 3a,b) while EKE is more concentrated around the separated Gulf Stream and North Atlantic Current region (Fig. 3c,d). One may notice that MTDE is negative, which has to do with buoyancy always taking negative values due to ρ_0 used in MITgcm. Conceptually, MTDE can be viewed as a well of potential energy. In the subsections below, we examine the time series of volume-averaged energy cycle. Spatial maps of the terms in the MKE and EKE budgets are given in Figs. A1 and A4 respectively.

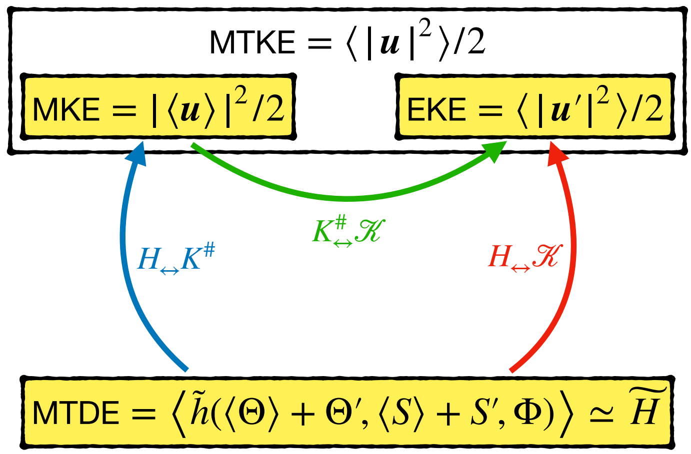

FIG. 2. A schematic of the ensemble Reynold's decomposition of the energy cycle using dynamic enthalpy formulation (neglecting the external forcing and diabatic terms). The ensemble-mean total kinetic energy (MTKE) is easily split into kinetic energy of the mean (MKE) and kinetic energy of the eddies (EKE). The ensemble-mean total dynamic enthalpy (MTDE) cannot be split, but may be simplified if $\langle \tilde{b} \rangle \simeq \tilde{b}(\langle \Theta \rangle, \langle S \rangle, \Phi)$. In this case the interaction terms, $H_{\leftrightarrow}K^{\#}$ (in blue font) and $H_{\leftrightarrow}\mathscr{K}$ (in red font), can be written explicitly, i.e. (15) and (16).

a. Entire model domain

We show in Fig. 4 the time series of MTDE, EKE and MKE, along with the energy exchange between the reservoirs volume-averaged over the entire domain (20°S - 55°N, 262°E - 348°E) and full water column. The magnitude of EKE is larger than MKE. EKE has two local maxima about March and November respectively while MKE seemingly lags one-to-two months behind EKE also with a dual peak. MTDE is orders of magnitude larger than MKE and EKE, which is consistent with our notion that most of the dynamical energy in the ocean is stored as potential energy.

Shifting our attention to Fig. 4b, the energy input from MTDE to EKE takes its maximum during March, which is similar to $\langle w'b^{\dagger} \rangle$, implying that baroclinic instability is active during boreal winter. The similarity implies that there is only a small amount of net eddy influx of DE fluctuation ($\nabla \cdot \langle \boldsymbol{v}'h^{\dagger} \rangle \lesssim 0$) at the north and south open boundaries of our domain at 20°S and 55°N. Energy input from EKE from MKE is also positive year around although with two local maxima around February and August - October respectively. Although noisy, energy from MTDE is fluxed to MKE for most of the year with largest values during March, and is two orders of magnitude larger than the energy fluxes to EKE (cf. Fig. A3). The EKE and MKE advective influx from the boundaries

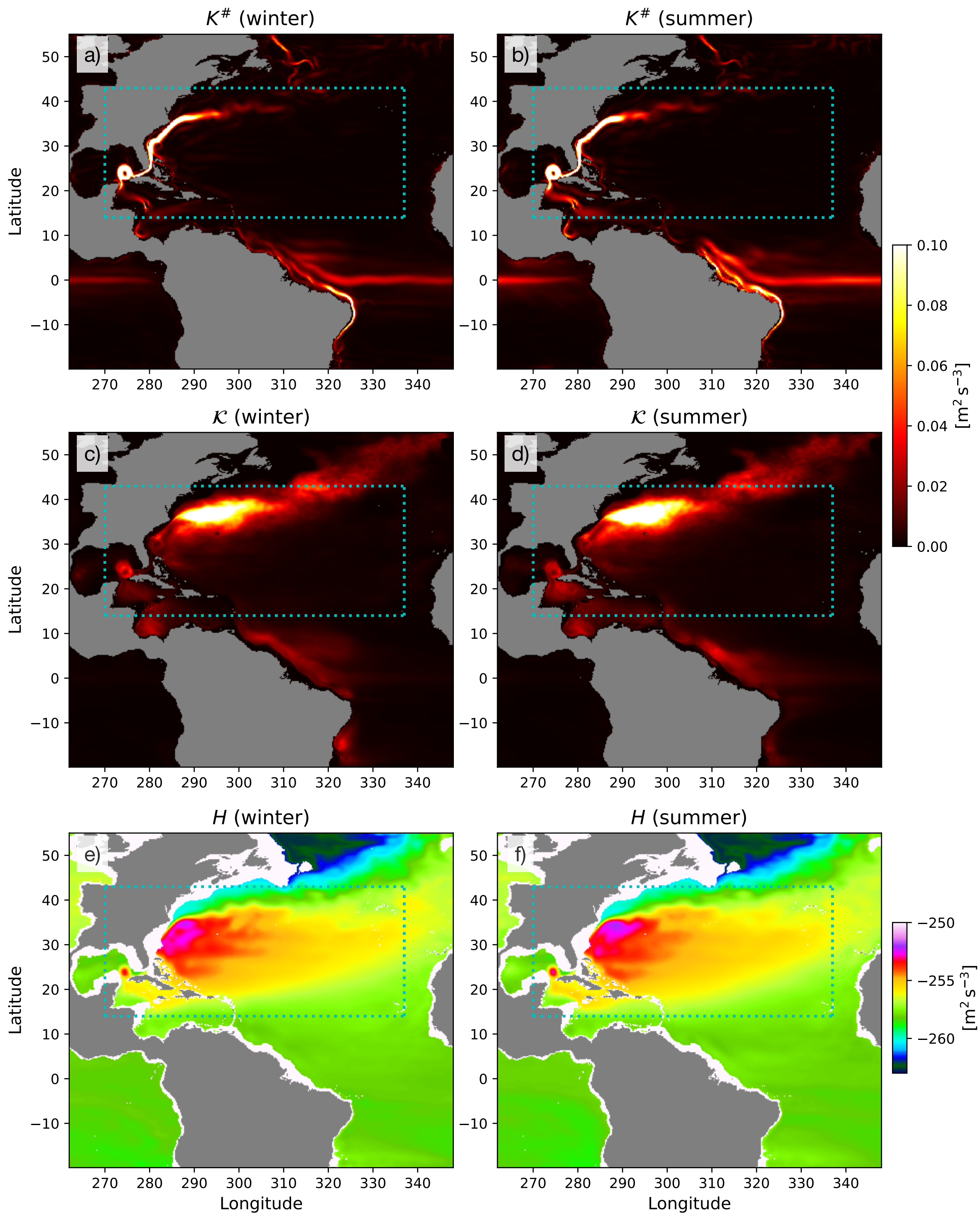

FIG. 3. MKE and EKE vertically averaged over the top 1000 m for winter (Jan.-Mar.) and summer (Jul.-Sep.) (a-d) of 1967. MTDE, also averaged over the top 1000 m, for each season (e,f). The subdomain considered for the wind-driven gyre in Section 3b is indicated with the cyan dotted lines.

(i.e. $-\langle \boldsymbol{v} \cdot \nabla \mathscr{K} \rangle$ and $-\left[\langle \boldsymbol{v} \rangle \cdot \nabla K^{\#} + \nabla \cdot \left\langle \boldsymbol{v}'(\langle \boldsymbol{u} \rangle \cdot \boldsymbol{u}')\right\rangle\right]$ respectively) are negligible compared to the flux between the energy reservoirs and exhibit no seasonality (grey-solid curves in Fig. 4b and f). $H_{\leftrightarrow}K^{\#}$ is roughly two orders of magnitude larger than the other terms shown in the right column of Fig. 4 but the mean vertical pressure work cancels it out (not shown) leaving the mean horizontal pressure work as the net contribution ($-\langle \boldsymbol{u} \rangle \cdot \nabla_{\mathrm{h}} \langle \phi \rangle$; cf. Fig. A1b and c). Another interesting thing to note is the existence of two local maxima in both the EKE and $K^{\#}_{\leftrightarrow}\mathscr{K}$ timeseries. The dual peak in the two timeseries seemingly implies that the energy input from MKE to EKE (sometimes associated with barotropic instability) is dominating over baroclinic instability in modulating the temporal variability of EKE. The magnitude of $K^{\#}_{\leftrightarrow}\mathscr{K}$ (green-solid curve in Fig. 4b) being larger than $H_{\leftrightarrow}\mathscr{K}$ (red-solid curve in Fig. 4b) later into the year also corroborates our argument.

Energy input from forcing, largely due to wind stress, to MKE is consistently positive ($\langle \boldsymbol{u} \rangle \cdot \langle \boldsymbol{\mathcal{F}} \rangle > 0$) while it tends to damp out the eddies ($\langle \boldsymbol{u}' \cdot \boldsymbol{\mathcal{F}}' \rangle < 0$), although the latter is smaller by two orders of magnitude than the former (cf. Figs. A1d and A4d). The eddy killing effect by wind stress and thermal feedback is consistent with recent findings (Renault et al. 2016, 2023), albeit severely underestimated here due to us prescribing absolute wind stress instead of relative. We remind the reader that CheapAML follows the COARE3 prescription for wind forcing that enters the momentum equations (Fairall et al. 2003) and hence $\langle \boldsymbol{u}' \cdot \boldsymbol{\mathcal{F}}' \rangle$ has a weak dependence on sea-surface temperature fluctuations even when absolute wind stress is prescribed. Dissipation is consistently a sink for KE and takes the largest magnitude in winter, viz. $\langle \boldsymbol{u} \rangle \cdot \langle \boldsymbol{\varepsilon} \rangle$. EKE dissipation $\langle \boldsymbol{u}' \cdot \boldsymbol{\varepsilon}' \rangle$ tends to mirror $H_{\leftrightarrow}\mathscr{K}$ and $\langle w' b^{\dagger} \rangle$. The fact that dissipation (here estabilished by harmonic and biharmonic numerical viscosity) is a leading order term for EKE may indicate a forward cascade of KE particularly during boreal winter.

b. Wind-driven gyre

We now focus on the subdomain of 270°E - 337°E and 14°N - 43°N and upper 1000 m as the region of wind-driven gyre, a domain somewhat similar to Jamet et al. (2020b). The wind-driven gyre imprints itself onto MTDE as a shoaling of the potential energy well (Fig. 3e,f). The domain-averaged timeseries show that EKE roughly doubles MKE and takes its maximum around August / September while MKE exhibits a more pronounced dual peak. MTDE is in sync with EKE (Fig. 5a).

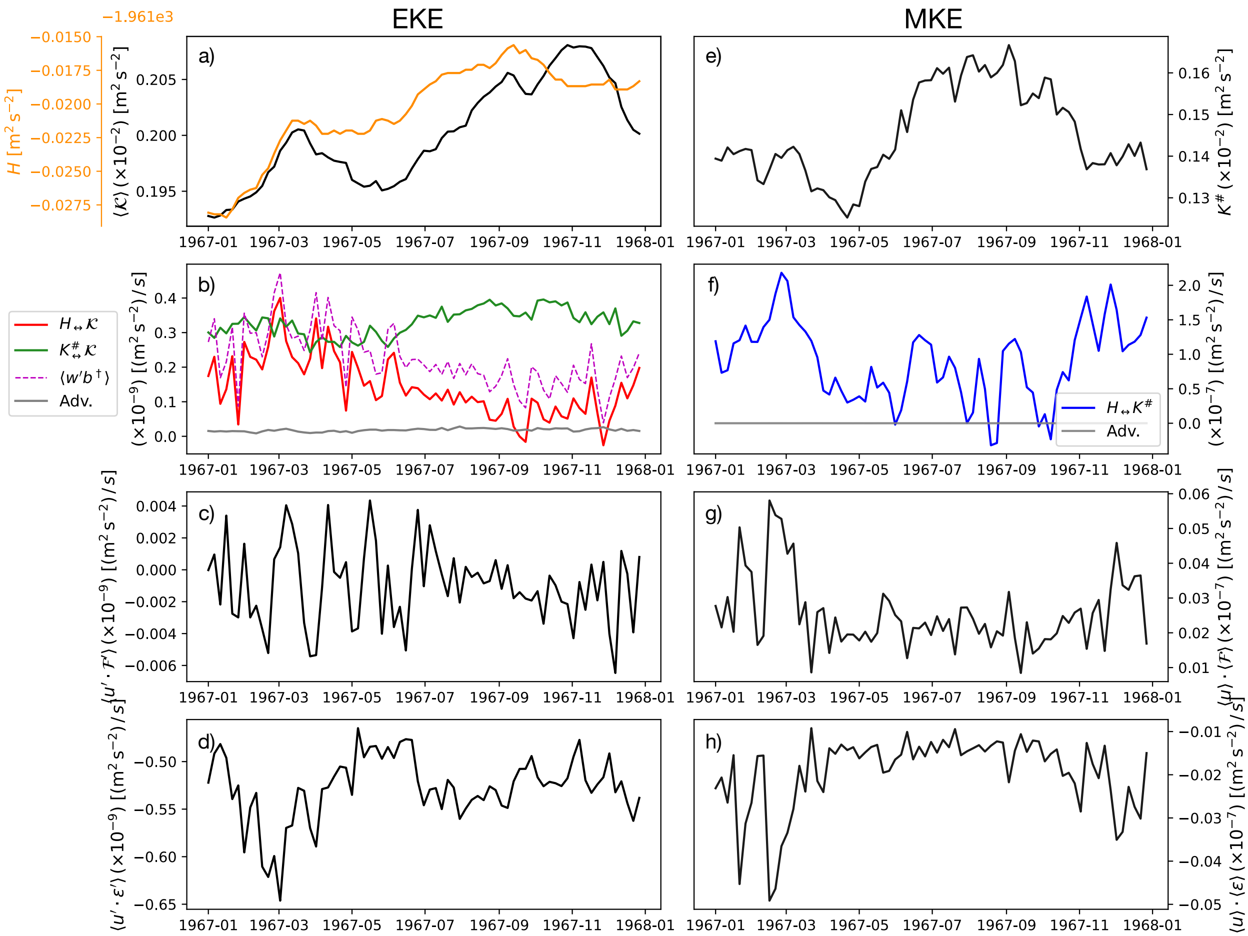

FIG. 4. Time series of the volume-averaged energy stored in each reservoir and non-divergent terms in the KE budget. EKE ($\mathscr{K}$) and MKE ($K^{\#}$) are plotted against the left (a - d) and right (e - h) panels respectively. MTDE (H) is plotted against the left y axis in orange in panel a. The exchange between MTDE and EKE ($H_{\leftrightarrow}\mathscr{K}$; solid-red curve) and MKE and EKE ($K^{\#}_{\leftrightarrow}\mathscr{K}$; solid-green curve) and eddy vertical buoyancy flux (magenta-dashed curve) are plotted in panel b while MTDE and MKE ($H_{\leftrightarrow}K^{\#}$; blue-solid curve) is plotted in panel f. Colors representing the energy flux between reservoirs in panels b and f correspond to Fig. 2. The contribution from the advective terms ($-\langle \boldsymbol{v} \cdot \nabla \mathscr{K} \rangle$ and $-\left[\langle \boldsymbol{v} \rangle \cdot \nabla K^{\#} + \nabla \cdot \left\langle \boldsymbol{v}' (\langle \boldsymbol{u} \rangle \cdot \boldsymbol{u}') \right\rangle\right]$) are in grey-solid curves (b, f). The diabatic terms, forcing and dissipation, are plotted in panels (c, g) and (d, h) respectively.

Unlike when averaged over the entire model domain, the energy flux from MTDE to EKE remains roughly twice as large as the eddy vertical buoyancy flux ($H_{\leftrightarrow}\mathscr{K} > \langle w'b^{\dagger} \rangle$; red-solid and magenta-dashed curves in Fig. 5b); the eddy outflux of DE fluctuation is non-negligible across the southern border at 14°N, viz. $\nabla \cdot \langle \boldsymbol{v}' h^{\dagger} \rangle > 0$ (cf. (10)), and remains relatively constant throughout the year. The relative magnitude between $H_{\leftrightarrow}\mathscr{K}$ and $\langle w'b^{\dagger} \rangle$ was insensitive to zonal and vertical expansion of the subdomain and extension northward (not shown). The energy flux from MTDE to MKE ($H_{\leftrightarrow}K^{\#}$) tends to change sign, indicating an occasional steepening of isopycnals in the mean flow. It is again canceled out by the mean vertical pressure work in closing the MKE budget (not shown). Unlike the eddy flux of DE fluctuation, the influx of KE into the subdomain due to advection is negligible for both the eddy and mean flow (grey solid and blue dashed curves in Fig. 5b).

Interestingly, similar to Fig. 4, the energy flux from MKE to EKE becomes larger than the eddy vertical buoyancy flux over the summer and autumn (green-solid and magenta-dashed curves in Fig. 5b), which implies that locally, barotropic processes are still the regulating mechanism over baroclinic. The KE maximum during boreal summer and autumn in western boundary current regions (e.g. the Kuroshio and Gulf Stream) has been observed in nature and is often explained as the time lag for the submesoscale eddies energized by winter-time baroclinic instability within the surface mixed layer to locally cascade upscale to the mesoscale (e.g. Zhai et al. 2008; Sasaki et al. 2014; Uchida et al. 2017; Dong et al. 2020). Our results imply that seasonality in the separated Gulf Stream is also modulated strongly by the eddy flux divergence of DE fluctuation from the region and a local KE transfer from the mean flow to eddies; the significance of the latter mechanism ($K^{\#}_{\leftrightarrow}\mathscr{K}$) is consistent with Uchida et al. (2021b) who diagnosed the energy cycle from a seasonally forced quasi-geostrophic double-gyre ensemble.

Regarding the diabatic terms, the relative contribution of viscous dissipation increases compared to when averaged over the full water column (Figs. 4d and 5d), which is attributable to KPP in the surface mixed layer. EKE dissipation tends to mirror $\langle w'b^{\dagger} \rangle$ with comparable magnitude (magenta-dashed curve in Fig. 5b and black solid curve in Fig. 5d), implying that much of the conversion from potential to kinetic energy due to baroclinic instability is lost locally to dissipation. Dissipation, a driver for a forward cascade of EKE at our model resolution (Molemaker et al. 2010; Arbic et al. 2013), again peaks during boreal winter, consistent with the seasonality found by Contreras et al. (2023).

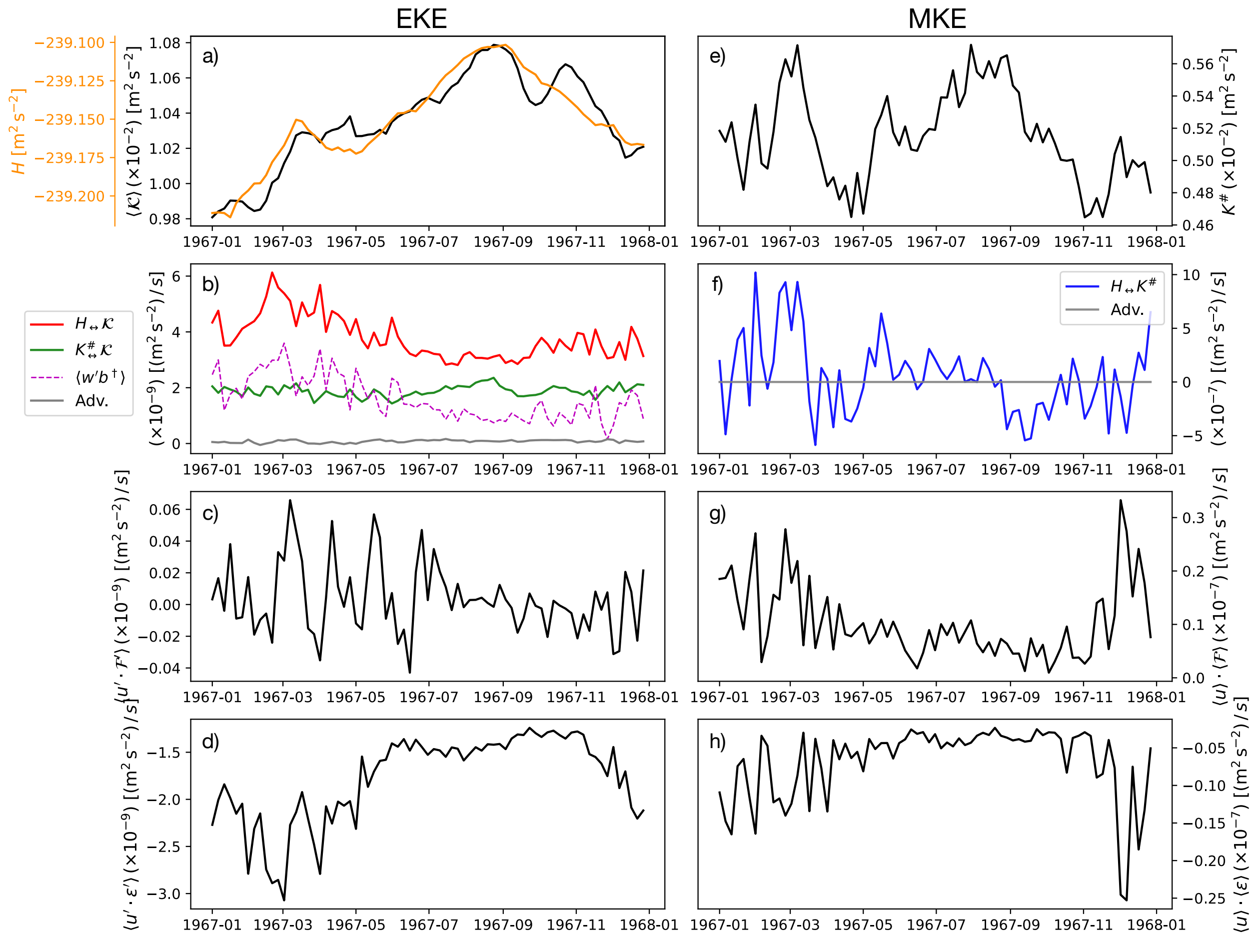

FIG. 5. Same as Fig. 4 but for the subdomain of wind-driven gyre. The subdomain is shown in Fig. 3 with the cyan dotted lines.

4. Conclusions and discussion

In this study, we have showcased the ocean energy cycle within the ensemble framework and geopotential coordinates (as opposed to isopycnal coordinates). To our knowledge, our study is novel in that we: i) decompose the mean and eddy energy reservoirs about the ensemble dimension for the ocean energy cycle, and ii) diagnose the potential energy in energy cycles via dynamic enthalpy (DE). The ensemble dimension being orthogonal to the space-time dimensions provides a parameter-free definition of eddy-mean flow decomposition, and preserves the non-stationary nature of the energy pathways, which we have addressed by examining the timeseries of the energy cycle. While the adoption of DE as potential energy is relatively scarce in the oceanographic literature (e.g. Jamet et al. 2020a), perhaps attributable to its computationally intensive nature, we have: i) argued that it is a natural and dynamically consistent extension of gravitational potential energy for a non-linear equation of state (EOS) and its independence from a reference state of stratification provides a level of objectivity in how potential energy is defined (Young 2010), and ii) documented its utility in the energy cycle.

One bewildering aspect, which naturally results from using DE, is that the potential energy reservoir can no longer be split into its mean and eddy components and the mean total dynamic enthalpy (MTDE) directly interacts with the mean kinetic energy (MKE) and eddy kinetic energy (EKE) reservoirs. This is a stark contrast to Lorenz (1955) where the potential energy reservoir available to eddies is a quadratic term and can be explicitly identified. We argue that this discrepancy is due to the fact that quasi geostrophy corresponds to the thickness-weighted averaged primitive equations of motion in isopycnal coordinates, and not the unweighted equations in geopotential coordinates (Marshall et al. 2012; Maddison and Marshall 2013; Meunier et al. 2023). Any dynamically consistent quantity resembling APE analogous to the quadratic form in quasi geostrophy under a non-linear EOS arises only upon thickness-weighted averaging the governing equations (cf. Aoki 2014; Loose et al. 2022; Uchida et al. 2022b, their Appendix A)

By examining the temporal variability of the energy cycle, we have demonstrated that in addition to the well-acknowledged mechanism of baroclinic instability local in space ($\langle w' b^\dagger \rangle$) in modulating its seasonality (e.g. Sasaki et al. 2014; Kang et al. 2016; Uchida et al. 2017; Dong et al. 2020), the non-local eddy transport of DE fluctuation ($\langle \boldsymbol{v}' h^\dagger \rangle$) and local transfer from MKE to EKE ($K^{\#}_{\leftrightarrow}\mathscr{K}$) could also be significant factors in the western boundary current regions, here, the separated Gulf Stream (Figs. 4, 5 and A4). In particular, the significance of non-local eddy flux of DE fluctuation is consistent with recent studies demonstrating that non-local transport of potential vorticity is crucial for a proper jet formation in wind-driven gyres (Uchida et al. 2022a; Deremble et al. 2023). $K^{\#}_{\leftrightarrow}\mathscr{K}$ being first-order importance amongst the energy pathways between energy reservoirs is consistent with (Jamet et al. 2020a, their Table 2) where they exhibited that the energy input to the mean flow by wind stress was lost to the eddies substantially via barotropic processes in the subtropical North Atlantic. It is also consistent with Uchida et al. (2021b) where they showed that barotropic pathways to the EKE reservoir can overtake baroclinic pathways under increased summertime stratification.

Future work involves: i) extending the time frame of analysis beyond 1967 for a robust seasonal cycle, ii) investigating how the energy cycle would differ when the equations of motion are thickness weighted (e.g. Bleck 1985; Aiki and Richards 2008; Loose et al. 2022; Uchida et al. 2022b), and iii) analyzing ocean ensembles with higher spatial resolution (currently under production; Uchida et al. 2023b, their Supplementary Material) to better resolve the effect of eddy dynamics on the energy cycle. In the context of climate, our framework is extendable straightforwardly to fully-coupled climate ensemble simulations (e.g. Maher et al. 2019; Romanou et al. 2023), which would allow us to quantify the temporally cumulative effect of anthropogenic carbon onto the ocean energy cycle and integrate it into the climate energy cycle as a whole (Deser et al. 2020).

Acknowledgments. This study is a contribution to the 'Assessing the Role of forced and internal Variability for the Ocean and climate Response in a changing climate' (ARVOR) project supported by the French 'Les Enveloppes Fluides et l'Environnement' (LEFE) program. W. Dewar is supported through NSF grants OCE-1829856, OCE-1941963 and OCE-2023585, and the French 'Make Our Planet Great Again' (MOPGA) program managed by the Agence Nationale de la Recherche under the Programme d'Investissement d'Avenir, reference ANR-18-MPGA-0002. The latter two grants served as the primary support for T. Uchida and partially for Q. Jamet. A. Poje acknowledges support from the NSF grant OCE-2123633. High-performance computing resources on Cheyenne (`doi:10.5065/D6RX99HX`) used for running the Chaocean ensemble of the North Atlantic were provided by NCAR's Computational and Information Systems Laboratory, sponsored by NSF, under the university large allocation UFSU0011. We would like to thank Edward Peirce and Kelly Hirai for maintaining the Florida State University cluster on which the data were analyzed. Upon getting his hands wet in producing realistic ensemble simulations, T. Uchida realized the formidable dedication it takes in doing so and is indebted to Q. Jamet for generating the Chaocean dataset. The MITgcm outputs were read using the `xmitgcm` Python package (Abernathey et al. 2022) and postprocessed with the `xgcm` Python package (Abernathey et al. 2021a).

Data availability statement. The simulation outputs are available on the Florida State University cluster (`http://ocean.fsu.edu/~qjamet/share/data/Uchida2021/`). The Jupyter notebooks used for diagnosing the model outputs are available via Github (`https://github.com/roxyboy/Energy_Zycle.git`; a DOI will be added upon acceptance of the manuscript).

APPENDIX

Energy cycle of non-thickness weighted primitive equations under geopotential coordinates

a. Energy budget of the eddy-mean flow

The ensemble-mean kinetic energy (MKE; $K^\# = |\langle \boldsymbol{u} \rangle|^2/2$) equation is given as

$$
\begin{aligned}
\frac{D^\#}{Dt} K^\# &= -\langle \boldsymbol{u} \rangle \cdot \nabla_\mathrm{h} \langle \phi \rangle - \langle u \rangle \nabla \cdot \langle \boldsymbol{v}' u' \rangle - \langle v \rangle \nabla \cdot \langle \boldsymbol{v}' v' \rangle + \langle \boldsymbol{u} \rangle \cdot \langle \boldsymbol{\mathcal{X}} \rangle \\
&= -\langle \boldsymbol{v} \rangle \cdot \nabla \langle \phi \rangle + \langle w \rangle \langle b \rangle - \underbrace{\left[\nabla \cdot \left\langle \boldsymbol{v}' (\langle \boldsymbol{u} \rangle \cdot \boldsymbol{u}') \right\rangle - \langle \boldsymbol{v}' \boldsymbol{u}' \rangle \cdot \nabla \langle \boldsymbol{u} \rangle \right]}_{= \langle u \rangle \nabla \cdot \langle \boldsymbol{v}' u' \rangle - \langle v \rangle \nabla \cdot \langle \boldsymbol{v}' v' \rangle} + \langle \boldsymbol{u} \rangle \cdot \langle \boldsymbol{\mathcal{X}} \rangle \, . \qquad \text{(A1)}
\end{aligned}
$$

The eddy-mean flow interaction term in (A1) is re-written in the form in square brackets because the divergence component vanishes upon a global volume integration. Figure A1 exhibits some of the terms in the MKE budget. The total kinetic energy (TKE), on the other hand, is

$$K_t + \boldsymbol{v} \cdot \nabla K = -\boldsymbol{u} \cdot \nabla_{\mathrm{h}} \phi + \boldsymbol{u} \cdot \boldsymbol{\mathcal{X}} . \tag{A2}$$

Now, TKE can be expanded as

$$\begin{aligned} K &= \frac{1}{2} |\langle \boldsymbol{u} \rangle + \boldsymbol{u}'|^2 \\ &= K^{\#} + \mathscr{K} + \langle \boldsymbol{u} \rangle \cdot \boldsymbol{u}' , \end{aligned} \tag{A3}$$

where $\mathscr{K} = |\boldsymbol{u}'|^2/2$ is the eddy kinetic energy (EKE) so

$$\begin{aligned} \langle \boldsymbol{v} \cdot \nabla K \rangle &= \Big\langle \big(\langle \boldsymbol{v} \rangle + \boldsymbol{v}' \big) \cdot \nabla \Big(K^{\#} + \mathscr{K} + \langle \boldsymbol{u} \rangle \cdot \boldsymbol{u}' \Big) \Big\rangle \\ &= \langle \boldsymbol{v} \rangle \cdot \nabla K^{\#} + \langle \boldsymbol{v} \cdot \nabla \mathscr{K} \rangle + \nabla \cdot \big\langle \boldsymbol{v}' (\langle \boldsymbol{u} \rangle \cdot \boldsymbol{u}') \big\rangle . \end{aligned} \tag{A4}$$

Hence, subtracting (A1) from the ensemble mean of (A2) yields

$$\langle \mathscr{K} \rangle_t = \underbrace{-\langle \boldsymbol{v}' \cdot \nabla \phi' \rangle + \langle w' b' \rangle}_{= -\langle \boldsymbol{u}' \cdot \nabla_{\mathrm{h}} \phi' \rangle} - \underbrace{\big(\langle \boldsymbol{v} \cdot \nabla \mathscr{K} \rangle + \langle \boldsymbol{u}' \boldsymbol{v}' \rangle \cdot \nabla \langle \boldsymbol{u} \rangle \big)}_{= \boldsymbol{u}' \cdot (\boldsymbol{v} \cdot \nabla \boldsymbol{u})'} + \langle \boldsymbol{u}' \cdot \boldsymbol{\mathcal{X}}' \rangle , \tag{A5}$$

where we see the mean flow and eddies exchanging energy via the term $-\langle \boldsymbol{u}' \boldsymbol{v}' \rangle \cdot \nabla \langle \boldsymbol{u} \rangle$, sometimes referred to as the shear-production term in the turbulence literature.

The Lagrangian tendency of dynamic enthalpy is (Young 2010)

$$h_t + \boldsymbol{v} \cdot \nabla h = \frac{Dh}{Dt} = -wb + \tilde{h}_{\Theta} \frac{D\Theta}{Dt} + \tilde{h}_S \frac{DS}{Dt} . \tag{A6}$$

The Lagrangian tendency in the latter two terms (equivalent to $\mathring{\Theta}$ and $\mathring{S}$ respectively) are, in theory, proportional to molecular and/or non-hydrostatic effects and diabatic forcing. In the manuscript, $\mathring{\Theta} = \mathring{S} = 0$ is assumed. The equation for mean total dynamic enthalpy (MTDE) becomes

$$\langle h \rangle_t + \langle \boldsymbol{v} \rangle \cdot \nabla \langle h \rangle = \frac{D^{\#}}{Dt} \langle h \rangle = -\langle w \rangle \langle b \rangle - \langle w' b' \rangle - \langle \boldsymbol{v}' \cdot \nabla h' \rangle + \big\langle \tilde{h}_{\Theta} \mathring{\Theta} \big\rangle + \big\langle \tilde{h}_S \mathring{S} \big\rangle . \tag{A7}$$

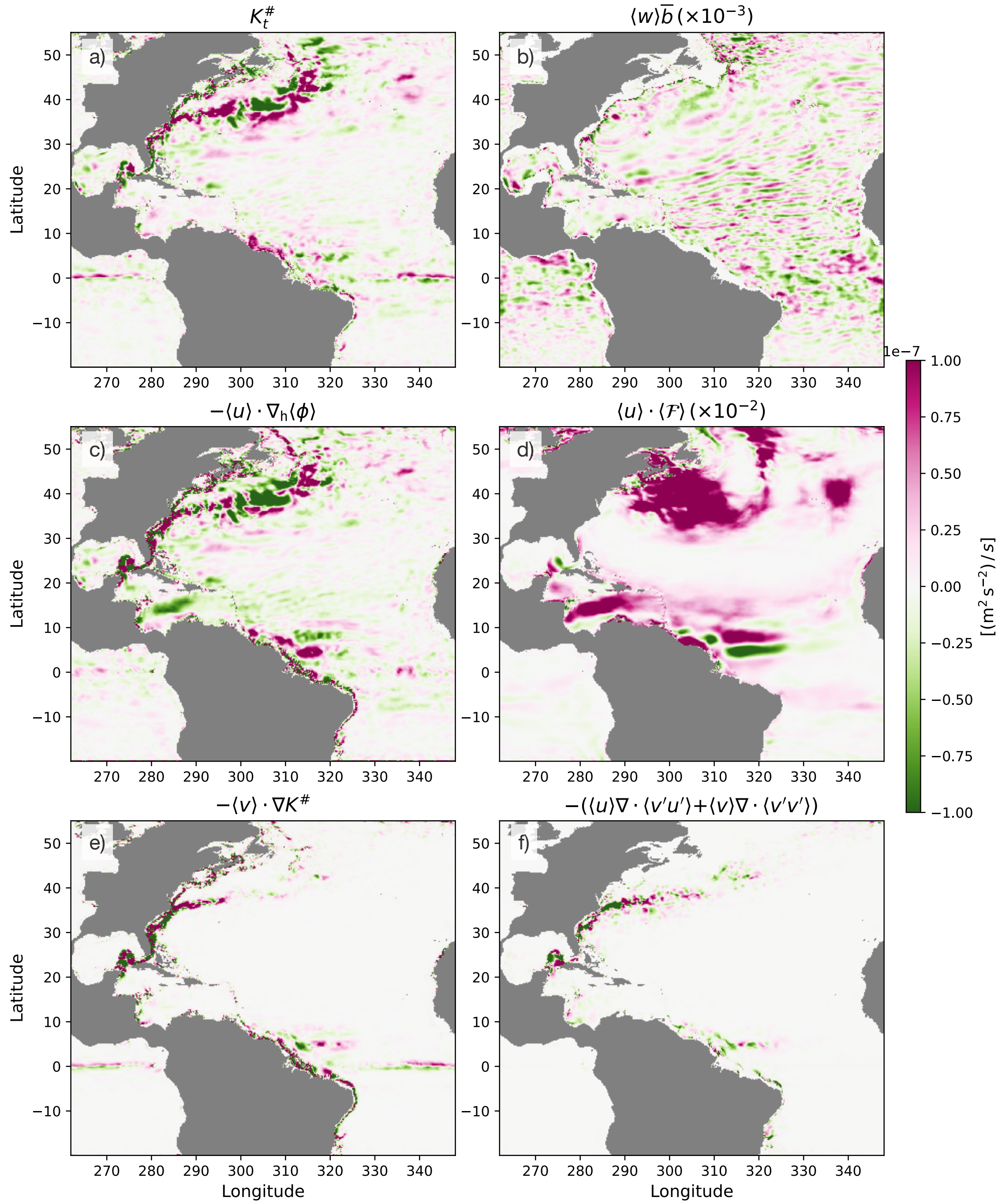

FIG. A1. The tendency of MKE (a), mean vertical buoyancy flux reduced by three orders of magnitude (b), horizontal pressure work (c), forcing reduced by two orders of magnitude (d), advection of MKE (e), and net loss to EKE (f) are shown for Jan. 1, 1967. The variables are vertically averaged over the top 1000 m except for the forcing, which only takes non-zero values at the surface.

Ensemble averaging (3) yields

$$\langle\tilde{h}\rangle = \int_{\Phi_0}^{\Phi} \frac{\langle\tilde{b}\rangle}{g}\, d\Phi^\dagger\,. \tag{A8}$$

Buoyancy in general is a thermodynamic variable, but the equation of state (EOS) is non-linear. Thus, we make use of a Taylor expansion as

$$\begin{aligned}
\langle\tilde{b}\rangle &= \left\langle \tilde{b}(\langle\Theta\rangle+\Theta', \langle S\rangle + S', \Phi)\right\rangle \\
&= \tilde{b}(\langle\Theta\rangle,\langle S\rangle,\Phi) + \tilde{b}_{\langle\Theta\rangle}(\langle\Theta\rangle,\langle S\rangle,\Phi)\langle\Theta'\rangle + \tilde{b}_{\langle S\rangle}(\langle\Theta\rangle,\langle S\rangle,\Phi)\langle S'\rangle \\
&\qquad + \tilde{b}_{\langle\Theta\rangle\langle\Theta\rangle}\frac{\langle\Theta'^2\rangle}{2} + \tilde{b}_{\langle\Theta\rangle\langle S\rangle}\langle\Theta' S'\rangle + \tilde{b}_{\langle S\rangle\langle S\rangle}\frac{\langle S'^2\rangle}{2} + \dots,
\end{aligned}$$

which argues for

$$\langle\tilde{b}\rangle = \widetilde{\overline{b}} + \widetilde{\mathcal{B}} \tag{A9}$$

where $\widetilde{\overline{b}} \stackrel{\text{def}}{=} \tilde{b}(\langle\Theta\rangle,\langle S\rangle,\Phi)$ and the terms with single-order pertubation vanish and $\widetilde{\mathcal{B}}$ is at most second order in perturbation because $\langle\Theta'\rangle = \langle S'\rangle = 0$. $\widetilde{\mathcal{B}}$ is only non-zero for a non-linear EOS and generally represents a small correction. Hence, MTDE becomes

$$\langle\tilde{h}\rangle = \int_{\Phi_0}^{\Phi} \frac{\widetilde{\overline{b}} + \widetilde{\mathcal{B}}}{g}\, d\Phi^\dagger \stackrel{\text{def}}{=} \widetilde{H} + \widetilde{\Lambda}, \tag{A10}$$

where $\widetilde{\Lambda} \stackrel{\text{def}}{=} g^{-1}\int_{\Phi_0}^{\Phi}\widetilde{\mathcal{B}}\, d\Phi^\dagger$ shoulders the non-linear effects and is ignored in (9). Buoyancy fluctuation, on the other hand, can be expanded as

$$\begin{aligned}
b' &= \tilde{b} - \langle\tilde{b}\rangle \\
&= \tilde{b}_{\langle\Theta\rangle}(\langle\Theta\rangle,\langle S\rangle,\Phi)\Theta' + \tilde{b}_{\langle S\rangle}(\langle\Theta\rangle,\langle S\rangle,\Phi)S' \\
&\qquad + \tilde{b}_{\langle\Theta\rangle\langle\Theta\rangle}\frac{\Theta'^2 - \langle\Theta'^2\rangle}{2} + \tilde{b}_{\langle\Theta\rangle\langle S\rangle}(\Theta' S' - \langle\Theta' S'\rangle) + \tilde{b}_{\langle S\rangle\langle S\rangle}\frac{S'^2 - \langle S'^2\rangle}{2} + \dots,
\end{aligned}$$

showing that it is approximated to second order by linear corrections. Thus,

$$b' = \tilde{b} - \left(\widetilde{\overline{b}} + \widetilde{\mathcal{B}}\right), \tag{A11}$$

$$h' = \tilde{h} - \left(\widetilde{H} + \widetilde{\Lambda}\right). \tag{A12}$$

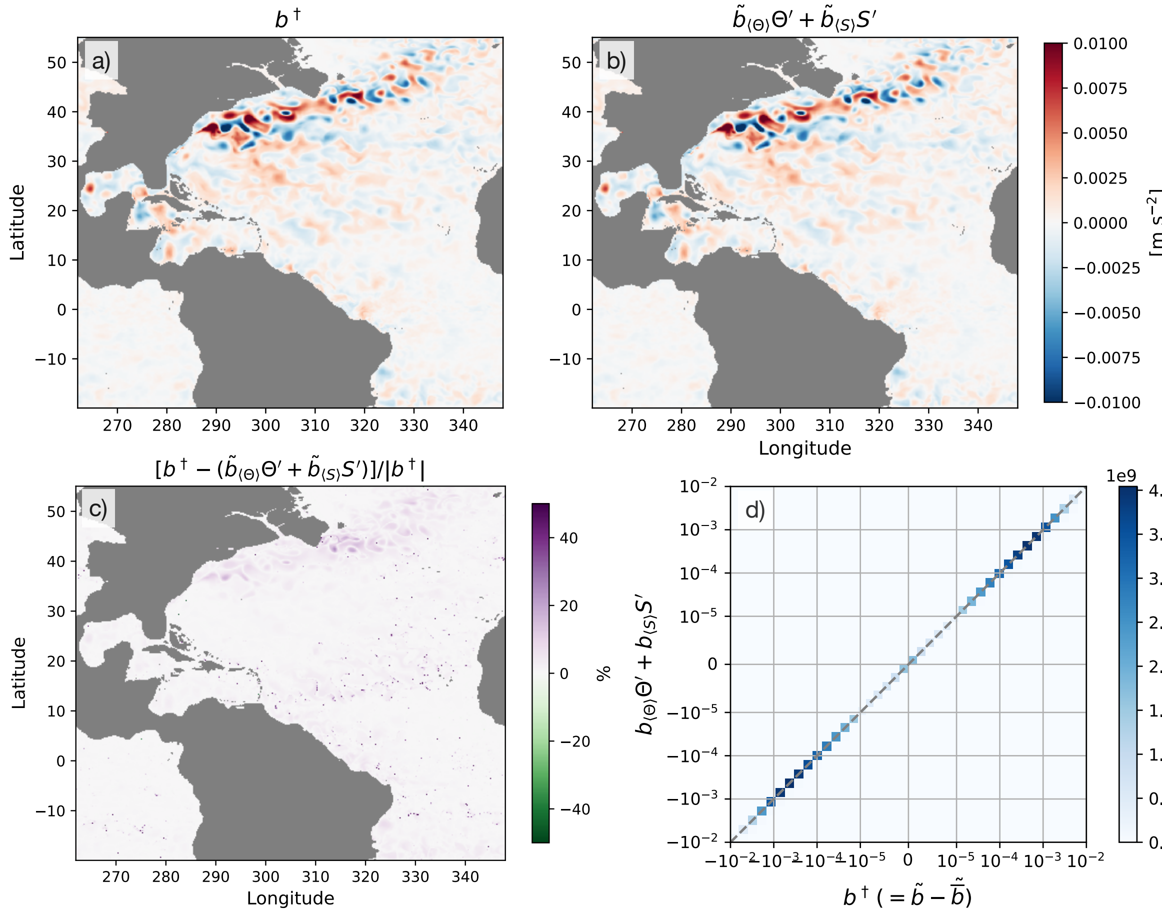

FIG. A2. Comparison between buoyancy fluctuation $\tilde{b}^\dagger (= \tilde{b} - \widetilde{\overline{b}})$ and $\tilde{b}_{\langle\Theta\rangle}(\langle\Theta\rangle, \langle S\rangle, \Phi)\Theta' + \tilde{b}_{\langle S\rangle}(\langle\Theta\rangle, \langle S\rangle, \Phi)S'$. The partial derivatives respective to mean potential temperature and practical salinity were taken using the `fastjmd95` Python package (Abernathey and Busecke 2020). The eddy buoyancy $b^\dagger$ (a), $\tilde{b}_{\langle\Theta\rangle}(\langle\Theta\rangle, \langle S\rangle, \Phi)\Theta' + \tilde{b}_{\langle S\rangle}(\langle\Theta\rangle, \langle S\rangle, \Phi)S'$ (b), their difference as a percentage (c) on January 1, 1967 at $z = -270$ m, and a joint histogram of the former two throughout 1967 over the entire three-dimensional domain is shown (d).

In view of (A9) - (A12), (A7) can be re-written as

$$\underbrace{\widetilde{H}_\Phi \frac{D^\#}{Dt}\Phi + \widetilde{H}_{\langle\Theta\rangle}\frac{D^\#}{Dt}\langle\Theta\rangle + \widetilde{H}_{\langle S\rangle}\frac{D^\#}{Dt}\langle S\rangle}_{=\frac{D^\#}{Dt}H} + \frac{D^\#}{Dt}\Lambda = -\langle w\rangle\langle b\rangle - \langle w'b'\rangle - \langle \boldsymbol{v}'\cdot\nabla(h-\Lambda)\rangle + \left\langle \tilde{h}_\Theta \mathring{\Theta}\right\rangle + \left\langle \tilde{h}_S \mathring{S}\right\rangle$$

$$= -\langle w\rangle(\overline{b} + \mathcal{B}) - \langle w'(b - \mathcal{B})\rangle$$

$$- \langle \boldsymbol{v}'\cdot\nabla(h-\Lambda)\rangle + \left\langle \tilde{h}_\Theta \mathring{\Theta}\right\rangle + \left\langle \tilde{h}_S \mathring{S}\right\rangle ,$$

$$\therefore\ \widetilde{H}_{\langle\Theta\rangle}\frac{D^{\#}}{Dt}\langle\Theta\rangle+\widetilde{H}_{\langle S\rangle}\frac{D^{\#}}{Dt}\langle S\rangle+\frac{D^{\#}}{Dt}\Lambda=-\langle w\rangle\mathscr{B}-\langle w'(b-\mathscr{B})\rangle-\langle\boldsymbol{v}'\cdot\nabla(h-\Lambda)\rangle\,, \tag{A13}$$

where we have used $H_\Phi\frac{D^{\#}}{Dt}\Phi=-\langle w\rangle\overline{b}$. Realizing that $\frac{D^{\#}}{Dt}\langle\Theta\rangle=-\langle\boldsymbol{v}'\cdot\nabla\Theta'\rangle+\left\langle\mathring{\Theta}\right\rangle$ and $\frac{D^{\#}}{Dt}\langle S\rangle=-\langle\boldsymbol{v}'\cdot\nabla S'\rangle+\left\langle\mathring{S}\right\rangle$ yields

$$\begin{aligned}\langle w'(b-\mathscr{B})\rangle=&-\frac{D^{\#}}{Dt}\Lambda-\langle w\rangle\mathscr{B}-\langle\boldsymbol{v}'\cdot\nabla(h-\Lambda)\rangle+\widetilde{H}_{\langle\Theta\rangle}\langle\boldsymbol{v}'\cdot\nabla\Theta'\rangle+\widetilde{H}_{\langle S\rangle}\langle\boldsymbol{v}'\cdot\nabla S'\rangle\\&+\left(\left\langle\tilde{h}_\Theta\mathring{\Theta}\right\rangle-\widetilde{H}_{\langle\Theta\rangle}\left\langle\mathring{\Theta}\right\rangle\right)+\left(\left\langle\tilde{h}_S\mathring{S}\right\rangle-\widetilde{H}_{\langle S\rangle}\left\langle\mathring{S}\right\rangle\right).\end{aligned} \tag{A14}$$

Equation (A14) allows us to unify the EKE and MTDE equations

$$\begin{aligned}\frac{D^{\#}}{Dt}(\langle\mathscr{K}\rangle+\Lambda)=&-\left\langle\boldsymbol{v}'\cdot\nabla\left[\phi'+\mathscr{K}+(h-\Lambda)\right]\right\rangle-\langle\boldsymbol{v}'\boldsymbol{u}'\rangle\cdot\nabla\langle\boldsymbol{u}\rangle+\langle\boldsymbol{u}'\cdot\boldsymbol{\mathcal{X}}'\rangle-\langle w\rangle\mathscr{B}\\&+\widetilde{H}_{\langle\Theta\rangle}\langle\boldsymbol{v}'\cdot\nabla\Theta'\rangle+\widetilde{H}_{\langle S\rangle}\langle\boldsymbol{v}'\cdot\nabla S'\rangle+\left(\left\langle\tilde{h}_\Theta\mathring{\Theta}\right\rangle-\widetilde{H}_{\langle\Theta\rangle}\left\langle\mathring{\Theta}\right\rangle\right)+\left(\left\langle\tilde{h}_S\mathring{S}\right\rangle-\widetilde{H}_{\langle S\rangle}\left\langle\mathring{S}\right\rangle\right).\end{aligned} \tag{A15}$$

On the other hand, the unifed MKE and MTDE equation becomes

$$\begin{aligned}\frac{D^{\#}}{Dt}\Big(K^{\#}+\underbrace{\langle h\rangle-\Lambda}_{=H}\Big)=&-\langle\boldsymbol{v}\rangle\cdot\nabla\langle\phi\rangle-\left[\nabla\cdot\left\langle\boldsymbol{v}'(\langle\boldsymbol{u}\rangle\cdot\boldsymbol{u}')\right\rangle-\langle\boldsymbol{v}'\boldsymbol{u}'\rangle\cdot\nabla\langle\boldsymbol{u}\rangle\right]+\langle\boldsymbol{u}\rangle\cdot\langle\boldsymbol{\mathcal{X}}\rangle+\langle w\rangle\mathscr{B}\\&-\left(\widetilde{H}_{\langle\Theta\rangle}\langle\boldsymbol{v}'\cdot\nabla\Theta'\rangle+\widetilde{H}_{\langle S\rangle}\langle\boldsymbol{v}'\cdot\nabla S'\rangle\right)-\left(\left\langle\tilde{h}_\Theta\mathring{\Theta}\right\rangle-\widetilde{H}_{\langle\Theta\rangle}\left\langle\mathring{\Theta}\right\rangle\right)+\left(\left\langle\tilde{h}_S\mathring{S}\right\rangle-\widetilde{H}_{\langle S\rangle}\left\langle\mathring{S}\right\rangle\right).\end{aligned} \tag{A16}$$

It appears that there is an additional energy reservoir stemming from the non-linearities in EOS but we remind the reader that an evolution equation for $\widetilde{\Lambda}$ (and $\widetilde{\mathscr{B}}$) cannot be formulated based on b' because $\tilde{b}-\langle\tilde{b}\rangle\neq\tilde{b}-\overline{\overline{\tilde{b}}}$. Furthermore, the quadratic terms in $\mathscr{B}$ (e.g. $\tilde{b}_{\langle\Theta\rangle\langle\Theta\rangle}\frac{\langle\Theta'^2\rangle}{2}$) may appear analogous to APE but under a linear EOS, APE would be proportional to $\left\langle(\tilde{b}_{\langle\Theta\rangle}\Theta')^2\right\rangle$; $\tilde{b}_{\langle\Theta\rangle\langle\Theta\rangle}\frac{\langle\Theta'^2\rangle}{2}$ is a term tapping into the internal energy of thermodynamics and is generally much smaller than $\left\langle(\tilde{b}_{\langle\Theta\rangle}\Theta')^2\right\rangle$.

In practice, we neglect all the second and higher-order correction terms and $b'\simeq\tilde{b}^{\dagger}\overset{\text{def}}{=}\tilde{b}-\overline{\overline{\tilde{b}}}$ in this manuscript. Subsequently, we adopt $\langle\tilde{h}\rangle\overset{\text{def}}{=}\widetilde{H}$ and $h'\simeq\tilde{h}^{\dagger}\overset{\text{def}}{=}\tilde{h}-\widetilde{H}$. The latter is used to diagnose $\nabla\cdot\langle\boldsymbol{v}'h^{\dagger}\rangle$. We show in Fig. A2 that b' approximated by $\tilde{b}-\overline{\overline{\tilde{b}}}$ and $\tilde{b}_{\langle\Theta\rangle}(\langle\Theta\rangle,\langle S\rangle,\Phi)\Theta'+\tilde{b}_{\langle S\rangle}(\langle\Theta\rangle,\langle S\rangle,\Phi)S'$ are nearly identical with each other across the year throughout the basin;

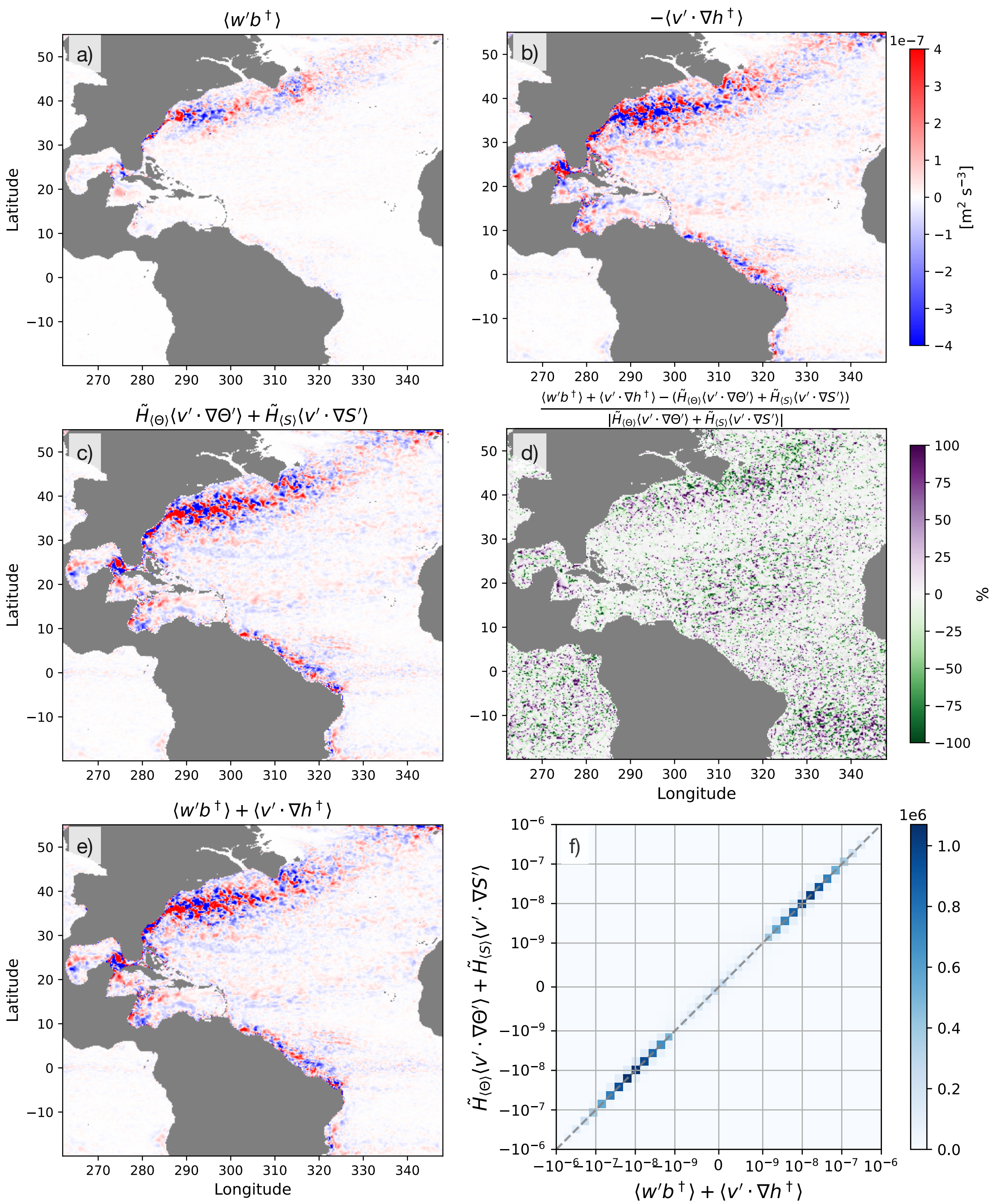

Fig. A3. Comparison of approximations to $H_{\leftrightarrow\mathscr{K}}$ on January 1, 1967. The vertical eddy buoyancy flux (a), convergence of eddy dynamic enthalpy flux (b), contribution due to convergence of eddy temperature and salinity flux (c), difference between the left- and right-hand side of (10) in percentage (d), net eddy buoyancy flux (e) all at $z = -270$ m, and a joint histogram over the entire three-dimensional domain (f). Panels a-c and e are plotted against the same colorbar. The ratio in panel d can be ill defined where the dominator is small.

the differences are largely contained within the separated Gulf Stream region. Equation (A14) can be simplified by dropping the terms due to diabatic nature and non-linearity in EOS, which leaves us with (10). Figure A3 demonstrates that (10) holds surprisingly well; we show a histogram exhibiting that the two align mostly along a one-to-one line (Fig. A3f). The end result of neglecting the non-linearity in the EOS and terms associated with diabatic mixing in (A15) and (A16) leaves us with (11), (12) and (13). There are two sources for eddy energy, one from the MKE and another from the MTDE field. The generalized pressure work tends to counteract the input from MTDE (Figs. A3 and A4).

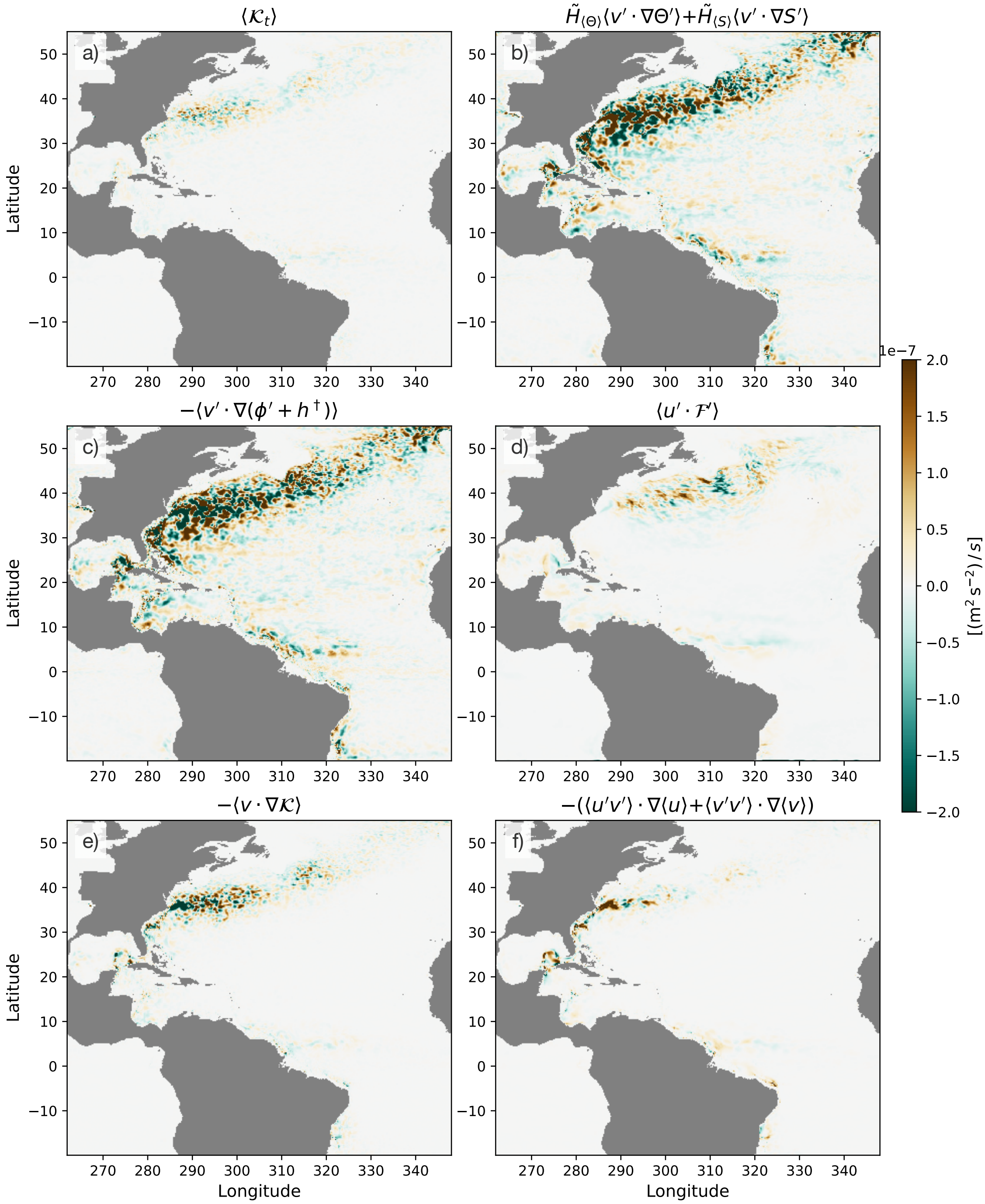

FIG. A4. The tendency of EKE (a), energy influx from MTDE (b), generalized pressure work (c), forcing (d), advection of EKE (e), and shear production (f) are shown for Jan. 1, 1967. The variables are vertically averaged over the top 1000 m except for the forcing, which only takes non-zero values at the surface. The influx from MTDE and generalized pressure work tend to counteract each other. $-\langle \boldsymbol{v}\cdot\nabla\mathscr{K}\rangle$ in panel e is diagnosed as $-\langle \boldsymbol{u}'\cdot(\boldsymbol{v}\cdot\nabla\boldsymbol{u})'\rangle+(\langle u'\boldsymbol{v}'\rangle\cdot\nabla\langle u\rangle+\langle v'\boldsymbol{v}'\rangle\cdot\nabla\langle v\rangle)$.

References

Abernathey, R. P., and J. Busecke, 2020: `fastjmd95`: Numba implementation of Jackett & McDougall (1995) ocean equation of state. URL https://github.com/xgcm/fastjmd95, https://doi.org/10.5281/zenodo.4498376.

Abernathey, R. P., and Coauthors, 2021a: `xgcm`: General circulation model postprocessing with xarray. URL https://xgcm.readthedocs.io/en/latest/, https://doi.org/10.5281/zenodo.3634752.

Abernathey, R. P., and Coauthors, 2021b: `xhistogram`: Fast, flexible, label-aware histograms for numpy and xarray. URL https://xhistogram.readthedocs.io/en/latest/, https://doi.org/10.5281/zenodo.7095156.

Abernathey, R. P., and Coauthors, 2022: `xmitgcm`: Read mitgcm mds binary files into xarray. URL https://github.com/MITgcm/xmitgcm, https://doi.org/10.5281/zenodo.5139886.

Aiki, H., and K. Richards, 2008: Energetics of the global ocean: The role of layer-thickness form drag. *Journal of Physical Oceanography*, **38**, 1845–1869, https://doi.org/10.1175/2008JPO3820.1.

Aiki, H., X. Zhai, and R. J. Greatbatch, 2016: Energetics of the global ocean: The role of mesoscale eddies. *Indo-Pacific climate variability and predictability*, 109–134, https://doi.org/10.1142/9789814696623_0004.

Aoki, K., 2014: A constraint on the thickness-weighted average equation of motion deduced from energetics. *Journal of Marine Research*, **72**, 355–382, https://doi.org/10.1357/002224014815469886.

Aoki, K., A. Kubokawa, R. Furue, and H. Sasaki, 2016: Influence of eddy momentum fluxes on the mean flow of the Kuroshio Extension in a 1/10 Ocean General Circulation Model. *Journal of Physical Oceanography*, **46 (9)**, 2769–2784, https://doi.org/10.1175/JPO-D-16-0021.1.

Arbic, B. K., K. L. Polzin, R. B. Scott, J. G. Richman, and J. F. Shriver, 2013: On eddy viscosity, energy cascades, and the horizontal resolution of gridded satellite altimeter products. *Journal of Physical Oceanography*, **43 (2)**, 283–300, https://doi.org/10.1175/JPO-D-11-0240.1.

Bachman, S. D., B. Fox-Kemper, and F. O. Bryan, 2015: A tracer-based inversion method for diagnosing eddy-induced diffusivity and advection. *Ocean Modelling*, **86**, 1–14, https://doi.org/10.1016/j.ocemod.2014.11.006.

Bleck, R., 1985: On the conversion between mean and eddy components of potential and kinetic energy in isentropic and isopycnic coordinates. *Dynamics of atmospheres and oceans*, **9 (1)**, 17–37, https://doi.org/10.1016/0377-0265(85)90014-4.

Buzzicotti, M., B. Storer, H. Khatri, S. Griffies, and H. Aluie, 2023: Spatio-temporal coarse-graining decomposition of the global ocean geostrophic kinetic energy. *Journal of Advances in Modeling Earth Systems*, **15 (6)**, e2023MS003 693, https://doi.org/10.1029/2023MS003693.

Charney, J. G., and Coauthors, 1979: *Carbon dioxide and climate: a scientific assessment*. National Academy of Sciences, Washington, DC.

Chen, R., and G. R. Flierl, 2015: The contribution of striations to the eddy energy budget and mixing: Diagnostic frameworks and results in a quasigeostrophic barotropic system with mean flow. *Journal of Physical Oceanography*, **45 (8)**, 2095–2113, https://doi.org/10.1175/JPO-D-14-0199.1.

Contreras, M., L. Renault, and P. Marchesiello, 2023: Understanding energy pathways in the Gulf Stream. *Journal of Physical Oceanography*, **53 (3)**, 719–736, https://doi.org/10.1175/JPO-D-22-0146.1.

Demyshev, S. G., and O. A. Dymova, 2022: Analysis of the annual mean energy cycle of the Black Sea circulation for the climatic, basin-scale and eddy regimes. *Ocean Dynamics*, **72 (3-4)**, 259–278, https://doi.org/10.1007/s10236-022-01504-0.

Deremble, B., T. Uchida, W. K. Dewar, and R. M. Samelson, 2023: Eddy-mean flow interaction with a multiple scale quasi geostrophic model. *Earth ArXiv*, https://doi.org/10.31223/X5KD4B.

Deremble, B., N. Wienders, and W. K. Dewar, 2013: CheapAML: A simple, atmospheric boundary layer model for use in ocean-only model calculations. *Monthly Weather Review*, **141 (2)**, 809–821, https://doi.org/10.1175/MWR-D-11-00254.1.

Deser, C., and Coauthors, 2020: Insights from earth system model initial-condition large ensembles and future prospects. *Nature Climate Change*, **10 (4)**, 277–286, https://doi.org/10.1038/s41558-020-0731-2.

Dewar, W. K., R. Parfitt, and N. Wienders, 2022: Routine Reversal of the AMOC in an Ocean Model Ensemble. *Geophysical Research Letters*, e2022GL100117, https://doi.org/10.1029/2022GL100117.

Dewar, W. K., J. Schoonover, T. McDougall, and R. Klein, 2016: Semicompressible ocean thermodynamics and Boussinesq energy conservation. *Fluids*, **1 (2)**, 9.

Dong, J., B. Fox-Kemper, H. Zhang, and C. Dong, 2020: The seasonality of submesoscale energy production, content, and cascade. *Geophysical Research Letters*, **47 (6)**, e2020GL087 388.

Eden, C., 2015: Revisiting the energetics of the ocean in Boussinesq approximation. *Journal of Physical Oceanography*, **45 (3)**, 630–637, https://doi.org/10.1175/JPO-D-14-0072.1.

Fairall, C. W., E. F. Bradley, J. Hare, A. A. Grachev, and J. B. Edson, 2003: Bulk parameterization of air–sea fluxes: Updates and verification for the COARE algorithm. *Journal of climate*, **16 (4)**, 571–591.

Gnanadesikan, A., M.-A. Pradal, and R. Abernathey, 2015: Isopycnal mixing by mesoscale eddies significantly impacts oceanic anthropogenic carbon uptake. *Geophysical Research Letters*, **42 (11)**, 4249–4255.

Griffies, S. M., and Coauthors, 2015: Impacts on ocean heat from transient mesoscale eddies in a hierarchy of climate models. *Journal of Climate*, **28 (3)**, 952–977, https://doi.org/10.1175/JCLI-D-14-00353.1.

Guo, Y., S. Bishop, F. Bryan, and S. Bachman, 2022: A global diagnosis of eddy potential energy budget in an eddy-permitting ocean model. *Journal of Physical Oceanography*, **52 (8)**, 1731–1748, https://doi.org/10.1175/JPO-D-22-0029.1.

Hartmann, D., V. Ramanathan, A. Berroir, and G. Hunt, 1986: Earth radiation budget data and climate research. *Reviews of Geophysics*, **24 (2)**, 439–468, https://doi.org/10.1029/RG024i002p00439.

Hersbach, H., C. Peubey, A. Simmons, P. Berrisford, P. Poli, and D. Dee, 2015: ERA-20CM: A twentieth-century atmospheric model ensemble. *Quarterly Journal of the Royal Meteorological Society*, **141 (691)**, 2350–2375, https://doi.org/10.1002/qj.2528.

Jackett, D. R., and T. J. McDougall, 1995: Minimal adjustment of hydrographic profiles to achieve static stability. *Journal of Atmospheric and Oceanic Technology*, **12**, 381–389.

Jamet, Q., A. Ajayi, J. Le Sommer, T. Penduff, A. Hogg, and W. Dewar, 2020a: On energy cascades in general flows: A lagrangian application. *Journal of Advances in Modeling Earth Systems*, **12 (12)**, e2020MS002 090, https://doi.org/10.1029/2020MS002090.

Jamet, Q., B. Deremble, N. Wienders, T. Uchida, and W. K. Dewar, 2020b: On wind-driven energetics of subtropical gyres. *Journal of Advances in Modeling Earth Systems*, **13 (4)**, e2020MS002 329, https://doi.org/10.1029/2020MS002329.

Jamet, Q., W. K. Dewar, N. Wienders, and B. Deremble, 2019: Spatio-temporal patterns of chaos in the Atlantic Overturning Circulation. *Geophysical Research Letters*, doi: 10.1029/2019GL082552.

Jamet, Q., W. K. Dewar, N. Wienders, B. Deremble, S. Close, and T. Penduff, 2020c: Locally and remotely forced subtropical AMOC variability: A matter of time scales. *Journal of Climate*, **33 (12)**, 5155–5172, https://doi.org/10.1175/JCLI-D-19-0844.1.

Jamet, Q., S. Leroux, W. K. Dewar, T. Penduff, J. Le Sommer, J.-M. Molines, and J. Gula, 2022: Non-local eddy-mean kinetic energy transfers in submesoscale-permitting ensemble simulations. *Journal of Advances in Modeling Earth Systems*, https://doi.org/10.1029/2022MS003057.

Kang, D., E. N. Curchitser, and A. Rosati, 2016: Seasonal variability of the gulf stream kinetic energy. *Journal of Physical Oceanography*, **46 (4)**, 1189–1207, https://doi.org/10.1175/JPO-D-15-0235.1.

Knutti, R., M. A. Rugenstein, and G. C. Hegerl, 2017: Beyond equilibrium climate sensitivity. *Nature Geoscience*, **10 (10)**, 727–736, https://doi.org/10.1038/ngeo3017.

Large, W., J. McWilliams, and S. Doney, 1994: Oceanic vertical mixing: A review and a model with a nonlocal boundary layer parameterization. *Reviews of Geophysics*, **32**, 363–403.

Lenderink, G., A. Van Ulden, B. Van den Hurk, and E. Van Meijgaard, 2007: Summertime inter-annual temperature variability in an ensemble of regional model simulations: Analysis of the surface energy budget. *Climatic Change*, **81**, 233–247, https://doi.org/10.1007/s10584-006-9229-9.

Leroux, S., T. Penduff, L. Bessières, J.-M. Molines, J.-M. Brankart, G. Sérazin, B. Barnier, and L. Terray, 2018: Intrinsic and atmospherically forced variability of the AMOC: Insights from a large-ensemble ocean hindcast. *Journal of Climate*, **31 (3)**, 1183–1203, https://doi.org/10.1175/JCLI-D-17-0168.1.

Loose, N., S. Bachman, I. Grooms, and M. Jansen, 2022: Diagnosing scale-dependent energy cycles in a high-resolution isopycnal ocean model. *Journal of Physical Oceanography*, **53 (1)**, 157–176, https://doi.org/10.1175/JPO-D-22-0083.1.

Lorenz, E., 1955: Available potential energy and the maintenance of the general circulation. *Tellus*, 157–167.

Maddison, J. R., and D. Marshall, 2013: The Eliassen–Palm flux tensor. *Journal of Fluid Mechanics*, **729**, 69–102, https://doi.org/10.1017/jfm.2013.259.

Maher, N., and Coauthors, 2019: The Max Planck Institute Grand Ensemble: Enabling the exploration of climate system variability. *Journal of Advances in Modeling Earth Systems*, **11 (7)**, 2050–2069, https://doi.org/10.1029/2019MS001639.

Marshall, D., J. Maddison, and P. Berloff, 2012: A framework for parameterizing eddy potential vorticity fluxes. *Journal of Physical Oceanography*, **42**, 539–557.

Marshall, J., C. Hill, L. Perelman, and A. Adcroft, 1997: Hydrostatic, quasi-hydrostatic and non-hydrostatic ocean modelling. *Journal of Geophysical Research*, **102**, 5733–5753.

Masson-Delmotte, V., and Coauthors, 2021: *Climate change 2021: The physical science basis*, Contribution of working group I to the sixth assessment report of the intergovernmental panel on climate change, Vol. 2. Cambridge University Press Cambridge, UK, https://doi.org/10.1017/9781009157896.

Meunier, J., B. Miquel, and B. Gallet, 2023: A direct derivation of the Gent-McWilliams/Redi diffusion tensor from quasi-geostrophic dynamics. *Journal of Fluid Mechanics*, **963**, A22, https://doi.org/10.1017/jfm.2023.347.

Molemaker, M. J., and J. C. McWilliams, 2010: Local balance and cross-scale flux of available potential energy. *Journal of Fluid Mechanics*, **645**, 295–314, https://doi.org/10.1017/S0022112009992643.

Molemaker, M. J., J. C. McWilliams, and X. Capet, 2010: Balanced and unbalanced routes to dissipation in an equilibrated Eady flow. *Journal of Fluid Mechanics*, **654**, 35–63, https://doi.org/10.1017/S0022112009993272.

Nikiéma, O., and R. Laprise, 2013: An approximate energy cycle for inter-member variability in ensemble simulations of a regional climate model. *Climate Dynamics*, **41**, 831–852, https://doi.org/10.1007/s00382-012-1575-x.

Nycander, J., 2010: Horizontal convection with a non-linear equation of state: generalization of a theorem of paparella and young. *Tellus A: Dynamic Meteorology and Oceanography*, **62 (2)**, 134–137, https://doi.org/10.1111/j.1600-0870.2009.00429.x.

Renault, L., S. Masson, V. Oerder, F. Colas, and J. McWilliams, 2023: Modulation of the oceanic mesoscale activity by the mesoscale thermal feedback to the atmosphere. *Journal of Physical Oceanography*, https://doi.org/10.1175/JPO-D-22-0256.1.

Renault, L., M. J. Molemaker, J. Gula, S. Masson, and J. C. McWilliams, 2016: Control and stabilization of the gulf stream by oceanic current interaction with the atmosphere. *Journal of Physical Oceanography*, **46 (11)**, 3439–3453, https://doi.org/10.1175/JPO-D-16-0115.1.

Romanou, A., and Coauthors, 2023: Stochastic Bifurcation of the North Atlantic Circulation Under A Mid-Range Future Climate Scenario With The NASA-GISS ModelE. *Journal of Climate*, 1–49, https://doi.org/10.1175/JCLI-D-22-0536.1.

Saenz, J. A., R. Tailleux, E. D. Butler, G. O. Hughes, and K. I. Oliver, 2015: Estimating Lorenz's reference state in an ocean with a nonlinear equation of state for seawater. *Journal of Physical Oceanography*, **45 (5)**, 1242–1257, https://doi.org/10.1175/JPO-D-14-0105.1.

Sasaki, H., P. Klein, B. Qiu, and Y. Sasai, 2014: Impact of oceanic-scale interactions on the seasonal modulation of ocean dynamics by the atmosphere. *Nature Communications*, **5**, 1–8.

Sérazin, G., and Coauthors, 2017: A global probabilistic study of the ocean heat content low-frequency variability: Atmospheric forcing versus oceanic chaos. *Geophysical Research Letters*, **44 (11)**, 5580–5589, https://doi.org/10.1002/2017GL073026.

Sherwood, S., and Coauthors, 2020: An assessment of earth's climate sensitivity using multiple lines of evidence. *Reviews of Geophysics*, **58 (4)**, e2019RG000 678, https://doi.org/10.1029/2019RG000678.

Sui, C. H., K. M. Lau, W. K. Tao, and J. Simpson, 1994: The tropical water and energy cycles in a cumulus ensemble model. Part I: Equilibrium climate. *Journal of the Atmospheric Sciences*, **51 (5)**, 711–728, https://doi.org/10.1175/1520-0469(1994)051⟨0711:TTWAEC⟩2.0.CO;2.

Tailleux, R., 2013: Available potential energy and exergy in stratified fluids. *Annual Review of Fluid Mechanics*, **45**, 35–58, https://doi.org/10.1146/annurev-fluid-011212-140620.

Tailleux, R., 2016: Generalized patched potential density and thermodynamic neutral density: Two new physically based quasi-neutral density variables for ocean water masses analyses and circulation studies. *Journal of Physical Oceanography*, **46 (12)**, 3571–3584, https://doi.org/10.1175/JPO-D-16-0072.1.

Tailleux, R., and G. Wolf, 2023: On the links between neutral directions, buoyancy forces, energetics, potential vorticity, and lateral stirring in the ocean: A first-principles approach. *ArXiv*, https://doi.org/10.48550/arXiv.2202.00456.

Uchida, T., R. P. Abernathey, and K. S. Smith, 2017: Seasonality of eddy kinetic energy in an eddy permitting global climate model. *Ocean Modelling*, **118**, 41–58, https://doi.org/10.1016/j.ocemod.2017.08.006.

Uchida, T., D. Balwada, Q. Jamet, W. K. Dewar, B. Deremble, T. Penduff, and J. Le Sommer, 2023a: Cautionary tales from the mesoscale eddy transport tensor. *Ocean Modelling*, **182**, 102 172, https://doi.org/10.1016/j.ocemod.2023.102172.

Uchida, T., B. Deremble, W. K. Dewar, and T. Penduff, 2021a: Diagnosing the Eliassen-Palm flux from a quasi-geostrophic double gyre ensemble. *EarthCube Annual Meeting*, NSF, https://doi.org/10.5281/zenodo.5496375, URL https://earthcube2021.github.io/ec21_book/notebooks/ec21_uchida_etal/notebooks/TU_05_Diagnosing-the-Eliassen-Palm-flux-from-a-quasi-geostrophic-double-gyre-ensemble.html.

Uchida, T., B. Deremble, and T. Penduff, 2021b: The seasonal variability of the ocean energy cycle from a quasi-geostrophic double gyre ensemble. *Fluids*, **6 (6)**, 206, https://doi.org/10.3390/fluids6060206.

Uchida, T., B. Deremble, and S. Popinet, 2022a: Deterministic model of the eddy dynamics for a midlatitude ocean model. *Journal of Physical Oceanography*, https://doi.org/10.1175/JPO-D-21-0217.1.

Uchida, T., Q. Jamet, W. K. Dewar, D. Balwada, J. Le Sommer, and T. Penduff, 2022b: Diagnosing the thickness-weighted averaged eddy-mean flow interaction in an eddying North Atlantic ensemble: The Eliassen–Palm flux. *Journal of Advances in Modeling Earth Systems*, **14 (5)**, e2021MS002 866, https://doi.org/10.1029/2021MS002866.

Uchida, T., Q. Jamet, A. C. Poje, and W. K. Dewar, 2021c: An ensemble-based eddy and spectral analysis, with application to the Gulf Stream. *Journal of Advances in Modeling Earth Systems*, **14 (4)**, e2021MS002 692, https://doi.org/10.1029/2021MS002692.

Uchida, T., Q. Jamet, A. C. Poje, N. Wienders, and W. K. Dewar, 2023b: Wavelet-based wavenumber spectral estimate of eddy kinetic energy: Application to the North Atlantic. *EarthArXiv*, https://doi.org/10.31223/X5036Q.

Von Storch, J.-S., C. Eden, I. Fast, H. Haak, D. Hernández-Deckers, E. Maier-Reimer, J. Marotzke, and D. Stammer, 2012: An estimate of the Lorenz energy cycle for the world ocean based on the STORM/NCEP simulation. *Journal of Physical Oceanography*, **42 (12)**, 2185–2205, https://doi.org/10.1175/JPO-D-12-079.1.

Wunsch, C., 1981: *The Evolution of Physical Oceanography: Scientific Surveys in Honor of Henry Stommel*, chap. Low frequency variability of the sea, 342–374. MIT Press.

Wunsch, C., and R. Ferrari, 2004: Vertical mixing, energy, and the general circulation of the oceans. *Annual Review of Fluid Mechanics*, **36**, 281–314, https://doi.org/10.1146/annurev.fluid.36.050802.122121.

Xie, J., H. Liu, and P. Lin, 2023: A multifaceted isoneutral eddy transport diagnostic framework and its application in the Southern Ocean. *Journal of Advances in Modeling Earth Systems*, https://doi.org/10.1029/2023MS003728.

Xie, S.-P., Y. Kosaka, and Y. M. Okumura, 2016: Distinct energy budgets for anthropogenic and natural changes during global warming hiatus. *Nature Geoscience*, **9 (1)**, 29–33, https://doi.org/10.1038/ngeo2581.

Yang, P., Z. Jing, H. Wang, L. Wu, Y. Chen, and S. Zhou, 2022: Role of frictional processes in mesoscale eddy available potential energy budget in the global ocean. *Geophysical Research Letters*, **49 (13)**, e2021GL097 557, https://doi.org/10.1029/2021GL097557.

Yang, Y., R. Chen, G. R. Flierl, and H. Zhang, 2023: A diagnostic framework linking eddy flux ellipse with eddy-mean energy exchange. *Research Square*, https://doi.org/10.21203/rs.3.rs-2954176/v1.

Young, W., 2010: Dynamic enthalpy, conservative temperature, and the seawater Boussinesq approximation. *Journal of Physical Oceanography*, **40**, 394–400, https://doi.org/10.1175/2009JPO4294.1.

Zhai, X., R. J. Greatbatch, and J.-D. Kohlmann, 2008: On the seasonal variability of eddy kinetic energy in the gulf stream region. *Geophysical Research Letters*, **35 (24)**.